

Static and free vibration analysis of functionally graded carbon nanotube reinforced skew plates.

Enrique García-Macías^{a,*}, Rafael Castro-Triguero^b, Erick I. Saavedra Flores^c, Michael I. Friswell^d,
Rafael Gallego^e

^a*Department of Continuum Mechanics and Structural Analysis, School of Engineering, University of Seville, Camino de los Descubrimientos s/n, E-41092-Seville, Spain*

^b*Department of Mechanics, University of Cordoba, Campus de Rabanales, Cordoba, CP 14071, Spain*

^c*Departamento de Ingeniería en Obras Civiles, Universidad de Santiago de Chile, Av. Ecuador 3659, Santiago, Chile*

^d*Zienkiewicz Centre for Computational Engineering, College of Engineering, Swansea University, Singleton Park, SA2 8PP, United Kingdom*

^e*Dept. Structural Mechanics and Hydraulic Engineering, University of Granada, 18071 Granada, Spain*

Abstract

The remarkable mechanical and sensing properties of carbon nanotubes (CNTs) suggest that they are ideal candidates for high performance and self-sensing composites. However, the study of CNT-based composites is still under development. This paper provides results of static and dynamic numerical simulations of thin and moderately thick functionally graded (FG-CNTRC) skew plates with uniaxially aligned reinforcements. The shell element is formulated in oblique coordinates and based on the first-order shear deformation plate theory. The theoretical development rests upon the Hu-Washizu principle. Independent approximations of displacements (bilinear), strains and stresses (piecewise constant subregions) provide a consistent mechanism to formulate an efficient four-noded skew element with a total of twenty degrees of freedom. An invariant definition of the elastic transversely isotropic tensor is employed based on the representation theorem. The FG-CNTRC skew plates are studied for a uniform and three different distributions (two symmetric and one asymmetric) of CNTs. Detailed parametric studies have been carried out to investigate the influences of skew angle, CNT volume fraction, thickness-to-width ratio, aspect ratio and boundary conditions. In addition, the effects of fiber orientation are also examined. The obtained results are compared to the FE commercial package ANSYS and the limited existing bibliography with good agreement.

Keywords:

Vibration analysis, skew shells, Hu-Washizu functional, shell finite elements, uniaxially aligned CNT reinforcements, functionally graded material

1. Introduction

Since the discovery of carbon nanotubes (CNTs) by Ijima [1] in 1991, many researchers have investigated their unique capabilities as reinforcements in composite materials. Due to their remarkable mechanical, electrical and thermal properties, carbon nanotubes are considered ideal reinforcing fibers for advanced high strength materials and smart materials with self sensing capabilities [2, 3]. In actual structural applications, it is important to develop theoretical models in order to predict the response of structural elements made of carbon nanotube-reinforced composites (CNTRC). In particular, skew plates are widely employed in civil and aeronautical engineering applications such as panels in skew bridges, construction of wings, tails and fins of swept-wing aircraft, etc. However, due to the mathematical difficulties involved in their formulation, works on the static and dynamic analysis of CNTRC skew elements are scarce in the literature [4].

The number of publications dealing with static and dynamic analysis of CNTRC structural elements have increased considerably in recent years. Wuite and Adali [5] studied the bending behavior of classical symmetric cross-ply and angle-ply laminated beams reinforced by aligned CNTs and isotropic beams reinforced by randomly oriented CNTs. By using a micromechanical constitutive model based on the Mori-Tanaka method, they highlighted that small percentages of CNT reinforcement lead to significant improvement in beam stiffness. Vodenitcharova and Zhang [6] developed a continuum model for the uniform bending and bending-induced buckling of a straight nanocomposite beam with circular cross section reinforced by a single-walled carbon nanotube

*Corresponding author.

Email address: egarcia28@us.es (Enrique García-Macías)

(SWNT). The results showed that although the addition of a matrix to a SWNT increases the load carrying capacity, the thicker matrix layers the SWNT buckles locally at smaller bending angles and greater flattening ratios. Formica et al. [7] studied the vibrational properties of cantilevered CNTRC plates with an Eshelby-Mori-Tanaka approach and finite element modeling. The results demonstrated the ability of CNTs to tune the vibrational properties of composites and increase the fundamental frequencies up to 500%. These exceptional properties have motivated many researchers to optimize the contribution of CNTs. According to this principle, Arani et al. [8] investigated analytically and numerically the buckling behavior of CNTRC rectangular plates. Based on classical laminate plate theory and the third-order shear deformation theory for moderately thick plates, they optimized the orientation of CNTs to achieve the highest critical load. Another example of this interest is the research carried out by Rokni et al. [9]. By dividing a beam along its longitudinal and thickness direction with the inclusion proportion as the design variable, they proposed a new two-dimensional optimum distribution of reinforcements of a polymer composite micro-beams to maximize the fundamental natural frequency given a weight percentage of CNTs.

Functionally graded materials (FGMs) belong to a branch of advanced materials characterized by spatially varying properties. This concept has promoted the development of a wide range of applications of functionally graded composite materials since its origin in 1984 (see e.g. [10]). Inspired by this idea, Shen [11] proposed non-uniform distributions of CNTs within an isotropic matrix. In this work, nonlinear vibration of functionally graded CNT-reinforced composite (FG-CNTRC) plates in thermal environments was presented. Researchers have employed many different methodologies to model FG-CNTRCs and most of them are recorded in a recent review by Liew et al. [12]. Zhu et al. [13] carried out bending and free vibration analysis of FG-CNTRC plates by using a finite element model based on the first-order shear deformation plate theory (FSDT). Ke et al. [14] presented nonlinear free vibration analysis of FG-CNTRC beams within the framework of Timoshenko beam theory and Ritz method solved by a direct iterative technique. They concluded that symmetrical distributions of CNTs provide higher linear and nonlinear natural frequencies for FG-CNTRC beams than with uniform or unsymmetrical distribution of CNTs. Zhang et al. [15] proposed a meshless local Petrov-Galerkin approach based on the moving Kriging interpolation technique to analyze the geometrically nonlinear thermoelastic behavior of functionally graded plates in thermal environments. Shen and Zhang [16] analyzed the thermal buckling and postbuckling behavior of uniform and symmetric FG-CNTRC plates under in-plane temperature variation. These results showed that the buckling temperature as well as thermal postbuckling strength of the plate can be increased with functionally graded reinforcement. However, in some cases the plate with intermediate nanotube volume fraction may not present intermediate buckling temperature and initial thermal postbuckling strength. Aragh et al. [17] proposed an Eshelby-Mori-Tanaka approach and a 2-D generalized differential quadrature method (GDQM) to investigate the vibrational behavior of rectangular plates resting on elastic foundations. Yas and Heshmati used Timoshenko beam theory to analyze the vibration of straight uniform [18] and non-uniform [19] FG-CNTRC beams subjected to moving loads. Alibeigloo and Liew [20] studied the bending behavior of FG-CNTRC plates with simply supported edges subjected to thermo-mechanical loading conditions by three dimensional elasticity theory and using the Fourier series expansion and state-space method. This work was extended by Alibeigloo and Emtehani [21] for various boundary conditions by using the differential quadrature method. Zhang et al. [22] proposed a state-space Levy method for the vibration analysis of FG-CNT composite plates subjected to in-plane loads based on higher-order shear deformation theory. This research analyzed three different symmetric distributions of the reinforcements along the thickness, namely UD, FG-X and FG-O. They concluded that FG-X provides the largest frequency and critical buckling in-plane load. Whereas, the frequency for the FGO-CNT plate was the lowest. Wu and Li [23] used a unified formulation of Reissner's mixed variational theorem (RMVT) based finite prism methods (FPMs) to study the three-dimensional free vibration behavior of FG-CNTRC plates. Free vibration analyses of quadrilateral laminated plates were carried out by Malekzadeh and Zarei [24] using first shear deformation theory and discretization of the spatial derivatives by the differential quadrature method (DQM). Furthermore, mesh-free methods, employed in many different fields such as elastodynamic problems [25] and wave equations [26], have also been widely employed in the simulation of FG-CNTRCs. Zhang et al. [27] employed a local Kriging meshless method to evaluate the mechanical and thermal buckling behaviors of ceramic-metal functionally graded plates (FGPs). Lei et al. [28] presented parametric studies of the dynamic stability of CNTRC-FG cylindrical panels under static and periodic axial force using the mesh-free-kp-Ritz method and the Eshelby-Mori-Tanaka homogenization framework. Lei et al. [29] employed this methodology to carry out vibration analysis of thin-to-moderately thick laminated FG-CNT rectangular plates. Zhang and Liew [30] presented detailed parametric studies of the large deflection behaviors of quadrilateral FG-CNT for different types of CNT distributions. They showed that the geometric parameters such as side angle, thickness-to-width ratio or plate aspect ratios are more significant than material parameters such as CNT distribution and CNT volume fraction. Zhang et al. [31] employed the ILMS-Ritz method to assess the postbuckling behavior of FG-CNT plates with edges elastically restrained against translation and rotation under axial compression. Some other results can be found in the literature dealing with the buckling analysis of FG-CNTRC thick plates resting on Winkler [32] and Pasternak foundations

[33], free vibration analysis of triangular plates [34], cylindrical panels [35, 36], three-dimensional free vibration analysis of FG-CNTRC plates [37], vibration of thick functionally graded carbon nanotube-reinforced composite plates resting on elastic Winkler foundations [38], vibration analysis of functionally graded carbon nanotube reinforced thick plates with elastically restrained edges [30], etc.

In the case of skew plates, the verification of their mathematical formulation is difficult because of the lack of exact solutions, and those available in literature are based on approximate methods. Over the past four decades, a lot of research has been carried out on the study of isotropic skew plates [39–42]. In contrast, research work dealing with the analysis of anisotropic skew plates is rather scant, and even more so for FG-CNT composite materials. However, Zhang et al. [30] obtained the buckling solution of FG-CNT reinforced composite moderately thick skew plates using the element-free IMLS-Ritz method and first-order shear deformation theory (FSDT). The same authors [4] also provided approximate solutions for the free vibration of uniform and a symmetric distribution of the volume fraction of CNT in moderately thick FG-CNT skew plates. This methodology was also employed by Lei et al. [43] to perform buckling analysis of thick FG-CNT skew plates resting on Pasternak foundations. Geometrically nonlinear large deformation analysis of FG-CNT skew plates resting on Pasternak foundations was carried out by Zhang and Liew [44].

In this paper, we develop an efficient finite element formulation based on the Hu-Washizu principle to obtain approximate solutions for static and free vibration of various types of FG-CNTRC skew plates with moderate thickness. The shell theory is formulated in oblique coordinates and includes the effects of transverse shear strains by first-order shear deformation theory (FSDT). An invariant definition of the elastic transversely isotropic tensor based on the representation theorem is also defined in oblique coordinates. Independent approximations of displacements (bilinear), strains and stresses (piecewise constant within subregions) provide a consistent mechanism to formulate four-noded skew elements with a total of twenty degrees of freedom. A set of eigenvalue equations for the FG-CNTRC skew plate vibration is derived, from which the natural frequencies and mode shapes can be obtained. Detailed parametric studies have been carried out to investigate the influences of skew angle, carbon nanotube volume fraction, plate thickness-to-width ratio, plate aspect ratio, boundary conditions and the distribution profile of reinforcements (uniform and three non-uniform distributions) on the static and dynamic response of the FG-CNTRC skew plates. The results are compared to commercial codes and the limited existing bibliography with very good agreement.

2. Functionally graded CNTRC plates

Figure 1 shows the four types of FG-CNTRC skew plates considered in this paper, with length a , width b , thickness t and fiber orientation angle φ . UD-CNTRC represents the uniform distribution and FG-V, FG-O and FG-X CNTRC are the functionally graded distributions of carbon nanotubes in the thickness direction of the composite skew plates. The effective material properties of the two-phase nanocomposites mixture of uniaxially aligned CNTs reinforcements and a polymeric matrix, can be estimated according to the Mori-Tanaka scheme [45] or the rule of mixtures [3, 46]. The accuracy of the extended rule of mixtures (EROM) has been widely discussed and a remarkable synergism with the Mori-Tanaka scheme for functionally graded ceramic-metal beams is reported in [17]. Due to the simplicity and convenience, in the present study, the extended rule of mixture was employed by introducing the CNT efficiency parameters and the effective material properties of CNTRC skew plates can thus be written as [11]

$$E_{11} = \eta_1 V_{CNT} E_{11}^{CNT} + V_m E^m \quad (1a)$$

$$\frac{\eta_2}{E_{22}} = \frac{V_{CNT}}{E_{22}^{CNT}} + \frac{V_m}{E^m} \quad (1b)$$

$$\frac{\eta_3}{G_{12}} = \frac{V_{CNT}}{G_{12}^{CNT}} + \frac{V_m}{G^m} \quad (1c)$$

where E_{11}^{CNT} , E_{22}^{CNT} and G_{12}^{CNT} indicate the Young's moduli and shear modulus of SWCNTs, respectively, and E^m and G^m represent corresponding properties of the isotropic matrix. To account for the scale-dependent material properties, the CNT efficiency parameters, η_j ($j=1,2,3$), were introduced and can be calculated by matching the effective properties of the CNTRC obtained from a molecular dynamics (MD) or multi-scale simulations with those from the rule of mixtures. V_{CNT} and V_m are the volume fractions of the carbon nanotubes and matrix, respectively, and the sum of the volume fractions of the two constituents should equal unity. Similarly, the thermal expansion coefficients, α_{11} and α_{22} , in the longitudinal and transverse directions respectively, Poisson's ratio ν_{12} and the density ρ of the nanocomposite plates can be determined in the same way as

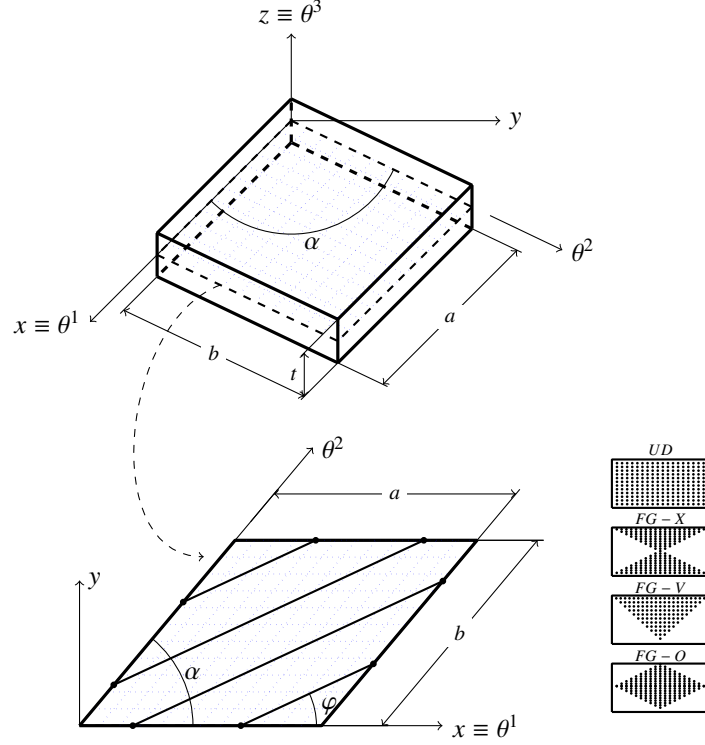


Figure 1: Geometry and configurations of the functionally graded carbon nanotube-reinforced (FG-CNTRC) skew plates.

$$\nu_{12} = V_{CNT}\nu_{12}^{CNT} + V_m\nu^m \quad (2a)$$

$$\rho = V_{CNT}\rho^{CNT} + V_m\rho^m \quad (2b)$$

$$\alpha_{11} = V_{CNT}\alpha_{11}^{CNT} + V_m\alpha^m \quad (2c)$$

$$\alpha_{22} = (1 + \nu_{12}^{CNT})V_{CNT}\alpha_{22}^{CNT} + (1 + \nu^m)V_m\alpha^m - \nu_{12}\alpha_{11} \quad (2d)$$

where ν_{12}^{CNT} and ν^m are Poisson's ratios, and α_{11}^{CNT} , α_{22}^{CNT} and α^m are the thermal expansion coefficients of the CNT and matrix, respectively. Note that ν_{12} is considered as constant over the thickness of the functionally graded CNTRC skew plates.

And the other effective mechanical properties are

$$\begin{aligned} E_{33} &= E_{22}, & G_{13} &= G_{12}, & G_{23} &= \frac{1}{2} \frac{E_{22}}{1+\nu_{23}}, \\ \nu_{13} &= \nu_{12}, & \nu_{31} &= \nu_{21}, & \nu_{32} &= \nu_{23} = \nu_{21}, \\ \nu_{21} &= \nu_{12} \frac{E_{22}}{E_{11}} \end{aligned} \quad (3)$$

The uniform and three types of functionally graded distributions of the carbon nanotubes along the thickness direction of the nanocomposite skew plates shown in Fig. 1 are assumed to be

$$\begin{aligned} V_{CNT} &= V_{CNT}^* & (\text{UD CNTRC}) \\ V_{CNT} &= \frac{4|z|}{t} V_{CNT}^* & (\text{FG-X CNTRC}) \\ V_{CNT} &= (1 + \frac{2z}{t}) V_{CNT}^* & (\text{FG-V CNTRC}) \\ V_{CNT} &= 2(1 - \frac{2|z|}{t}) V_{CNT}^* & (\text{FG-O CNTRC}) \end{aligned} \quad (4)$$

3. Finite element formulation

3.1. Parametrization of the geometry

Consider CNTRC skew plate of length a , width b , thickness t and skew angle α as shown in Fig. 1. The midsurface of the shell to be considered in this paper is given in terms of skew coordinates (θ^1, θ^2) , hence the

change of coordinates is given by

$$\begin{aligned} x &= \theta^1 + \theta^2 \cos \alpha \\ y &= \theta^2 \sin \alpha \\ z &= \theta^3 \end{aligned} \quad (5)$$

This parametrization leads a covariant basis \mathbf{a}_r defined by Eqs. (6)

$$\vec{a}_1 = \begin{Bmatrix} 1 \\ 0 \\ 0 \end{Bmatrix}, \quad \vec{a}_2 = \begin{Bmatrix} \cos \alpha \\ \sin \alpha \\ 0 \end{Bmatrix} \quad \text{and} \quad \vec{a}_3 = \begin{Bmatrix} 0 \\ 0 \\ 1 \end{Bmatrix} \quad (6)$$

The covariant metric tensor is noted by a has a value of $\sin^2 \alpha$ and leads a contravariant basis \mathbf{a}^r defined by Eqs. (7)

$$\vec{a}^1 = \begin{Bmatrix} 1 \\ -\tan^{-1} \alpha \\ 0 \end{Bmatrix}, \quad \vec{a}^2 = \begin{Bmatrix} 0 \\ \csc \alpha \\ 0 \end{Bmatrix} \quad \text{and} \quad \vec{a}^3 = \vec{a}_3 \quad (7)$$

3.2. Variational formulation, displacement field, stresses and strains of CNTRC skew plates

The theoretical formulation is derived by a variational formulation. Denoting by $\mathcal{U}(\gamma)$ the strain energy and by γ and σ the vectors containing the strain and stress components, respectively, a modified potential of Hu-Washizu assumes the form [47]

$$\Pi_{HW} [\mathbf{v}, \gamma, \sigma] = \int_V [\mathcal{U}(\gamma) - \sigma^T (\gamma - \mathbf{D} \mathbf{v}) - \Pi_b] dV - \int_{S_{\hat{v}}} (\mathbf{v} - \hat{\mathbf{v}}) \sigma \mathbf{n} dS - \int_{S_t} \Pi_t dS \quad (8)$$

In Eq. (8), \mathbf{v} and the index b represent the displacement vector and the body forces, respectively, whereas $\hat{\mathbf{v}}$ are prescribed displacements on the part of the boundary in which displacements are prescribed ($S_{\hat{v}}$).

The displacement field is constructed by first-order shear deformation. Hence the in-plane deformation $\gamma_{\alpha\beta}$ is expressed in terms of the extensional (${}_0\gamma_{\alpha\beta}$) and flexural (${}_1\gamma_{\alpha\beta}$) components of the Cauchy-Green strain tensor as

$$\gamma_{\alpha\beta} = {}_0\gamma_{\alpha\beta} + \theta^3 {}_1\gamma_{\alpha\beta}. \quad (9)$$

Denoting by V_α and V_3 the tangential displacements of the midsurface in the θ^α and θ^3 directions, and by ϕ_α the rotations about the θ^α lines, the strains in terms of the aforementioned displacements and rotations have the form

$$\text{Extensional strains : } {}_0\gamma_{\alpha\beta} = \frac{1}{2} (V_{\alpha\parallel\beta} + V_{\beta\parallel\alpha}), \quad (10a)$$

$$\text{Flexural strains : } {}_1\gamma_{\alpha\beta} = \frac{1}{2} (\sqrt{a} e_{\alpha\mu} \phi_{\parallel\beta}^\mu + \sqrt{a} e_{\beta\mu} \phi_{\parallel\alpha}^\mu), \quad (10b)$$

$$\text{Shear strains : } {}_2\gamma_{\alpha 3} = V_{3,\alpha} + \sqrt{a} e_{\alpha\mu} \phi^\mu \quad (10c)$$

In Eqs. (10) $e_{\alpha\beta}$ denote the permutation tensor associated with the undeformed surface and a double bar (\cdot) $_{\parallel}$ signifies covariant differentiation with respect to the undeformed surface. In vectorial form

$${}_0\gamma = \begin{Bmatrix} {}_0\gamma_{11} \\ {}_0\gamma_{22} \\ 2 {}_0\gamma_{12} \end{Bmatrix}, \quad {}_1\gamma = \begin{Bmatrix} {}_1\gamma_{11} \\ {}_1\gamma_{22} \\ 2 {}_1\gamma_{12} \end{Bmatrix} \quad \text{and} \quad \gamma_S = \begin{Bmatrix} \gamma_{13} \\ \gamma_{23} \end{Bmatrix} \quad (11)$$

The thin body assumption is considered in the z-direction, and thus it is often possible to neglect the transverse normal stress s^{33} . The stress-strain relationships are defined by

$$\begin{aligned} s^{\alpha\beta} &= \frac{\partial \Phi}{\partial \gamma_{\alpha\beta}} = C^{\alpha\beta\gamma\delta} \gamma_{\gamma\delta} \\ s^{\alpha 3} &= 2E^{\alpha 3\beta 3} \gamma_{\beta 3} \\ s^{33} &= 0 \end{aligned} \quad (12)$$

And the free-energy density takes the form

$$\Phi = \frac{1}{2} C^{\alpha\beta\gamma\delta} \gamma_{\alpha\beta} \gamma_{\gamma\delta} + 2 E^{\alpha\beta\beta} \gamma_{\alpha 3} \gamma_{\beta 3} \quad (13)$$

3.3. Linearly elastic transversely isotropic constitutive matrix in non-orthogonal coordinates

The definition of non-orthogonal coordinates requires a coherent definition of the stress-strain relationships. On the basis of the representation theorems of transversely isotropic tensors developed by Spencer [48], Lubarda and Chen [49] obtained the constitutive tensor of linear elastic transversely isotropic materials in a general coordinates system as

$$C_{ijkl} = \sum_{r=1}^6 c_r I_{ijkl}^r \quad (14)$$

The I^r are a set of linearly independent fourth order tensors that form a basis of an algebra of order 6 and the c_r are six elastic parameters. In component form, the fourth-order tensors I_r are defined by

$$I_{ijkl}^1 = \frac{1}{2}(a^{ik}a^{jl} + a^{il}a^{jk}) \quad (15a)$$

$$I_{ijkl}^2 = a^{ij}a^{kl} \quad (15b)$$

$$I_{ijkl}^3 = n_i n_j a^{kl} \quad (15c)$$

$$I_{ijkl}^4 = a^{ij} n_k n_l \quad (15d)$$

$$I_{ijkl}^5 = \frac{1}{2}(a^{ik}n_j n_l + a^{il}n_j n_k + a^{jk}n_i n_l + a^{jl}n_i n_k) \quad (15e)$$

$$I_{ijkl}^6 = n_i n_j n_k n_l \quad (15f)$$

where n_i are the rectangular components of a unit vector parallel to the axis of the transverse isotropy, defined in the mid-plane of the skew plate as $\vec{n} = (\cos \varphi, \sin \varphi, 0)$ (see Fig. 1), and a^{ij} are the components of the contravariant basis \mathbf{a}^r defined in Eq. (7). The material parameters, c_r , are defined as

$$\begin{aligned} c_1 &= 2\mu, & c_2 &= \lambda, & c_3 &= c_4 = \alpha, \\ c_5 &= 2(\mu_o - \mu), & c_6 &= \beta \end{aligned} \quad (16)$$

The material parameters c_r depend on five elastic constants: μ and λ , shear modulus within the plane of isotropy and the Lamé constant, the out-of-plane elastic shear modulus μ_o , α and β . In matrix notation the 4th order elasticity tensor of transversely isotropic material for a preferred x direction in a Cartesian coordinate system gives

$$C = \begin{bmatrix} 2\alpha + \beta + \lambda - 2\mu + 4\mu_o & \alpha + \lambda & \alpha + \lambda & 0 & 0 & 0 \\ \alpha + \lambda & \lambda + 2\mu & \lambda & 0 & 0 & 0 \\ \alpha + \lambda & \lambda & \lambda + 2\mu & 0 & 0 & 0 \\ 0 & 0 & 0 & \mu & 0 & 0 \\ 0 & 0 & 0 & 0 & \mu_o & 0 \\ 0 & 0 & 0 & 0 & 0 & \mu_o \end{bmatrix} \quad (17)$$

The relation between elastic invariant constants and the engineering constants can be found by comparing Eq. (17) with the classical transversely isotropic stiffness tensor. This comparison leads to

$$\alpha = \frac{E_{11}(E_{11} - E_{22})E_{22}\nu_{12}}{(E_{11} + E_{22}\nu_{12})(E_{11} - E_{22}\nu_{12}(1 + 2\nu_{12}))} \quad (18a)$$

$$\lambda = \frac{E_{11}E_{22}^2\nu_{12}(1 + \nu_{12})}{(E_{11} + E_{22}\nu_{12})(E_{11} - E_{22}\nu_{12}(1 + 2\nu_{12}))} \quad (18b)$$

$$\mu = \frac{E_{11}E_{22}}{2E_{11} + 2E_{22}\nu_{12}} \quad (18c)$$

$$\mu_o = G_{12} \quad (18d)$$

$$\beta = \frac{1}{2} \left(-8G_{12} + \frac{E_{11}E_{22}}{E_{11} + E_{22}\nu_{12}} + \frac{E_{11}(2E_{11} + E_{22} - 6E_{22}\nu_{12})}{E_{11} - E_{22}\nu_{12}(1 + 2\nu_{12})} \right) \quad (18e)$$

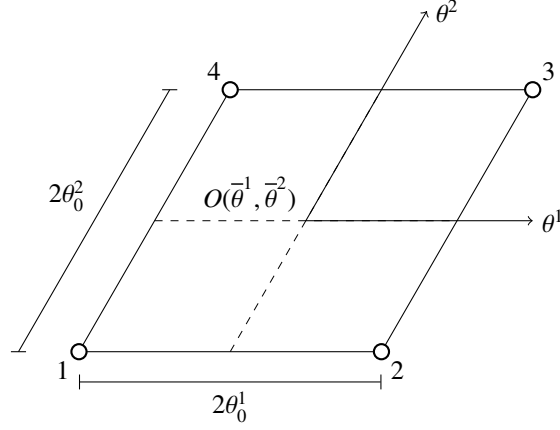


Figure 2: Four node skew quadrilateral shell finite element.

Once the constitutive tensor is obtained, the plane stress stiffness matrix can be obtained numerically by deleting the rows and columns associated with the z -direction in the compliance matrix. By inverting the resulting compliance matrix, the constitutive equations are written in Voigt's notation in the form

$$\begin{bmatrix} s_{11} \\ s_{22} \\ s_{12} \\ s_{23} \\ s_{13} \end{bmatrix} = \begin{bmatrix} Q_{11}(z) & Q_{12}(z) & 0 & 0 & 0 \\ Q_{12}(z) & Q_{22}(z) & 0 & 0 & 0 \\ 0 & 0 & Q_{66}(z) & 0 & 0 \\ 0 & 0 & 0 & Q_{44}(z) & 0 \\ 0 & 0 & 0 & 0 & Q_{55}(z) \end{bmatrix} \cdot \begin{bmatrix} \gamma_{11} \\ \gamma_{22} \\ \gamma_{12} \\ \gamma_{23} \\ \gamma_{13} \end{bmatrix} \quad (19)$$

$$\begin{aligned} (C_E^{ij}, C_C^{ij}, C_B^{ij}) &= \int_{-h/2}^{h/2} Q_{ij}(z) \cdot (1, z, z^2) dz \quad (i, j = 1, 2, 6), \\ C_S^{ij} &= \frac{1}{k_s} \int_{-h/2}^{h/2} Q_{ij} dz \quad (i, j = 4, 5) \end{aligned} \quad (20)$$

Note that Q_{ij} varies with z according to the grading profile of the CNTRC along the thickness. k_s denotes the transverse shear correction factor for FGM, given by [50]

$$k_s = \frac{6 - (\nu_i V_i + \nu_m V_m)}{5} \quad (21)$$

3.4. Stiffness matrix of skew plate element

The strain-energy density per unit of area at the reference surface can be defined by

$$U = \int_{-h/2}^{h/2} \Phi dz \quad (22)$$

From Eq. (9) and Eq. (13), the strain-energy density can be expressed as

$$U = \int_{-h/2}^{h/2} \left[\frac{1}{2} C^{\alpha\beta\gamma\delta} \left({}_0\gamma_{\alpha\beta} + \theta^3 {}_1\gamma_{\alpha\beta} \right) \left({}_0\gamma_{\gamma\delta} + \theta^3 {}_1\gamma_{\gamma\delta} \right) + 2 E^{\alpha\beta\beta} \gamma_{\alpha 3} \gamma_{\beta 3} \right] dz \quad (23)$$

Expression (23) for the strain energy can be represented as the sum of the extensional (U_E), bending (U_B), coupling (U_C) and transverse shear (U_S) strain energy as

$$\begin{aligned} U_{Total} &= U_E + U_B + U_C + U_S = \\ &= \frac{1}{2} \left({}_0\gamma^T \mathbf{C}_E {}_0\gamma + {}_1\gamma^T \mathbf{C}_B {}_1\gamma + {}_0\gamma^T \mathbf{C}_C {}_1\gamma + {}_1\gamma^T \mathbf{C}_C {}_0\gamma + \gamma_S^T \mathbf{C}_S \gamma_S \right) \end{aligned} \quad (24)$$

3.4.1. Discretization

The shell element derived in the present study is a four-noded skewed isoparametric finite element (see Fig. 2) with five degrees of freedom at each node: three physical components of the displacements u_1, u_2, u_3 and two components of the rotations φ_1, φ_2 Eq. (25). Bilinear shape functions N_k are chosen for the physical components of the displacements and rotations in the following way

$$u_i = \sum_{k=1}^4 u_i^k N_k \quad \text{and} \quad \varphi_\alpha = \sum_{k=1}^4 \varphi_\alpha^k N_k ; \quad (25)$$

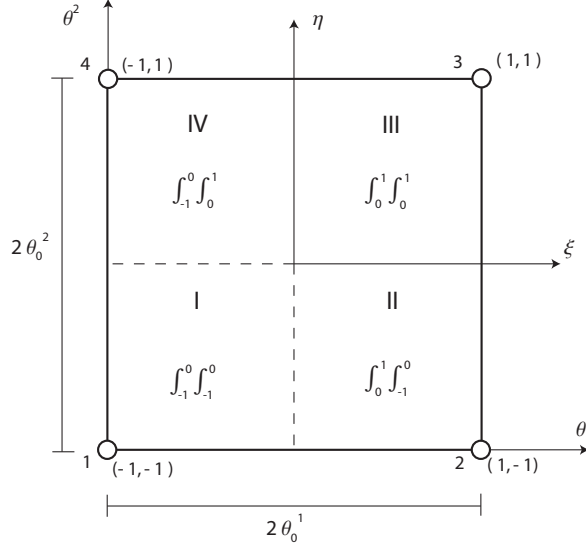


Figure 3: Subdomain areas throughout the finite element.

$$N_k = \frac{1}{4} (1 + \xi_k \xi) (1 + \eta_k \eta), \quad i = 1, 2, 3 \text{ and } \alpha = 1, 2. \quad (26)$$

As mentioned before, the use of the Hu-Washizu principle and the independent approximation of strain and stress yields a series of desirable features important for the reliability, convergence behavior, and efficiency of the elemental formulation such as the avoidance of superfluous energy and zero energy modes. Furthermore, the discrete approximation is drawn in a consistent manner from the general theory of the continuum and the mechanical behavior of the finite element, without resorting to special manipulations or computational procedures. In addition, it has been shown [47, 51, 52] that essential prerequisites for the achievement of these goals are: the identification of constant and higher-order deformational modes which are contained in the displacement/rotation assumptions, the realization that the constant terms are necessary for convergence, and that higher-order terms reappear in different strain components. Therefore, our approximation does not need to retain the higher-order terms in two different strain components (they are needed only to inhibit a mode).

For instance, the following assumptions for the extensional strains have been shown to serve the aforementioned goals

$$\begin{aligned} \gamma_{11} &= \bar{\gamma}_{11} + \bar{\bar{\gamma}}_{11} \eta, \\ \gamma_{22} &= \bar{\gamma}_{22} + \bar{\bar{\gamma}}_{22} \xi \\ \gamma_{12} &= \bar{\gamma}_{12} + \underline{\hat{\gamma}}_{11} \xi + \underline{\hat{\gamma}}_{22} \eta. \end{aligned} \quad (27)$$

Note that, according to the above ideas, the underlined terms in Eqs. (27) are not considered. The elimination of such terms allows the reduction of excessive internal energy and to improve convergence. Furthermore, the replacement of the linear variation of the strains and stresses by piecewise constant approximations leads to computational advantages that are most important in repetitive computations. The piecewise constant approximations can be improved by introducing four subdomains over the finite element (see Fig. 3). For example, Fig. 4 illustrates the piecewise approximation of γ_{11} and γ_{22} over two subdomains. The membrane shear strain γ_{12} is approximated by a constant.

Considering the piecewise approximations through the four subdomains and expressing strains in physical components (ε , κ , γ), the extensional, bending and shear strain over every subdomain are defined as

Extensional strains ($\varepsilon_{11}, \varepsilon_{22}, \varepsilon_{12}$)

$$\varepsilon_{11} = \begin{cases} \varepsilon_{11}^A & \text{in } A_I + A_{II} \\ \varepsilon_{11}^B & \text{in } A_{III} + A_{IV} \end{cases}, \quad \varepsilon_{22} = \begin{cases} \varepsilon_{22}^C & \text{in } A_I + A_{IV} \\ \varepsilon_{22}^D & \text{in } A_{II} + A_{III} \end{cases} \quad \text{and} \quad \varepsilon_{12} = \bar{\varepsilon}_{12} \quad \text{in } A \quad (28)$$

Bending strains ($\kappa_{11}, \kappa_{22}, \kappa_{12}$)

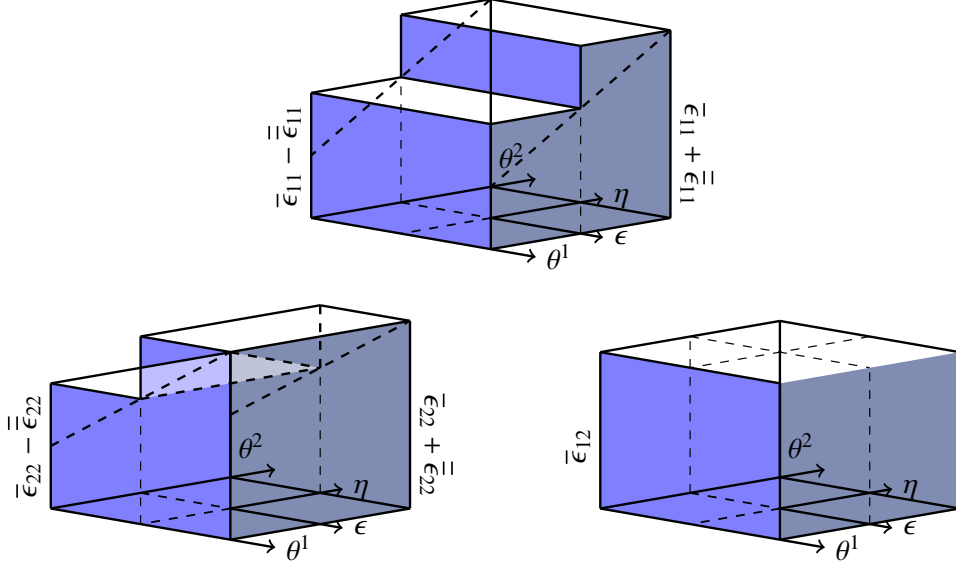


Figure 4: Schematic representation of the piecewise constant extensional strain approximation.

$$\kappa_{11} = \begin{cases} \kappa_{11}^A & \text{in } A_I + A_{II} \\ \kappa_{11}^B & \text{in } A_{III} + A_{IV} \end{cases}, \quad \kappa_{22} = \begin{cases} \kappa_{22}^C & \text{in } A_I + A_{IV} \\ \kappa_{22}^D & \text{in } A_{II} + A_{III} \end{cases} \quad \text{and} \quad \kappa_{12} = \bar{\kappa}_{12} \quad \text{in } A \quad (29)$$

Shear strains (γ_{13}, γ_{23})

$$\gamma_1 = \begin{cases} \gamma_1^A & \text{in } A_I + A_{II} \\ \gamma_1^B & \text{in } A_{III} + A_{IV} \end{cases} \quad \text{and} \quad \gamma_2 = \begin{cases} \gamma_2^C & \text{in } A_I + A_{IV} \\ \gamma_2^D & \text{in } A_{II} + A_{III} \end{cases} \quad (30)$$

As a consequence of this approximation, the strain energy term in the Hu-Washizu variational principle takes the form of

$$\int_A U dA = \int_{A_I} U_I dA + \dots + \int_{A_{IV}} U_{IV} dA = \sum_{i=I}^{IV} \int_{A_i} U_i dA = \frac{1}{2} \bar{\epsilon}^T \bar{\mathbf{D}}_E \bar{\epsilon} + \frac{1}{2} \bar{\kappa}^T \bar{\mathbf{D}}_B \bar{\kappa} + \frac{1}{2} \bar{\epsilon}^T \bar{\mathbf{D}}_C \bar{\kappa} + \frac{1}{2} \bar{\kappa}^T \bar{\mathbf{D}}_C \bar{\epsilon} + \frac{1}{2} \bar{\gamma}^T \bar{\mathbf{D}}_S \bar{\gamma} \quad (31)$$

where the vectors $\bar{\epsilon}$, $\bar{\kappa}$ and $\bar{\gamma}$ are defined by

$$\bar{\epsilon} = \begin{Bmatrix} \epsilon_{11}^A \\ \epsilon_{11}^B \\ \epsilon_{22}^C \\ \epsilon_{22}^D \\ 2\epsilon_{12} \end{Bmatrix}, \quad \bar{\kappa} = \begin{Bmatrix} \kappa_{11}^A \\ \kappa_{11}^B \\ \kappa_{22}^C \\ \kappa_{22}^D \\ 2\kappa_{12} \end{Bmatrix}, \quad \bar{\gamma} = \begin{Bmatrix} \gamma_1^A \\ \gamma_1^B \\ \gamma_2^C \\ \gamma_2^D \\ \gamma_2 \end{Bmatrix} \quad (32)$$

The matrices $\bar{\mathbf{D}}_E$, $\bar{\mathbf{D}}_B$, $\bar{\mathbf{D}}_C$ and $\bar{\mathbf{D}}_S$ are the discretized elasticity matrices that depend on the geometry of the surface —i.e., on the contravariant ($a^{\alpha\beta}$) and covariant ($a_{\alpha\beta}$) components of the metric tensors— and can be represented as follows

$$\bar{\mathbf{D}}_E = \begin{bmatrix} \int_{A_1+A_2} D_E(1,1) dA & 0 & \int_{A_1} D_E(1,2) dA & \int_{A_2} D_E(1,2) dA & \int_{A_1+A_2} D_E(1,3) dA \\ & \int_{A_3+A_4} D_E(1,1) dA & \int_{A_4} D_E(1,2) dA & \int_{A_3} D_E(1,2) dA & \int_{A_3+A_4} D_E(1,3) dA \\ & & \int_{A_1+A_4} D_E(2,2) dA & 0 & \int_{A_1+A_4} D_E(2,3) dA \\ \text{sym} & & & \int_{A_2+A_3} D_E(2,2) dA & \int_{A_2+A_3} D_E(2,3) dA \\ & & & & \int_A D_E(3,3) dA \end{bmatrix}, \quad (33)$$

$$\bar{\mathbf{D}}_S = \begin{bmatrix} \int_{A_1+A_2} D_S(1,1) dA & 0 & \int_{A_1} D_S(1,2) dA & \int_{A_2} D_S(1,2) dA \\ & \int_{A_3+A_4} D_S(1,1) dA & \int_{A_4} D_S(1,2) dA & \int_{A_3} D_S(1,2) dA \\ & \text{sym} & \int_{A_1+A_4} D_S(2,2) dA & 0 \\ & & & \int_{A_2+A_3} D_S(2,2) dA \end{bmatrix} \quad (34)$$

Furthermore, the parameters for the stress resultants are expressed by the following vector forms

$$\begin{aligned} \mathbf{N}^T &= [N_{11}^A \quad N_{11}^B \quad N_{22}^C \quad N_{22}^D \quad N_{12}] , \\ \mathbf{M}^T &= [M_{11}^A \quad M_{11}^B \quad M_{22}^C \quad M_{22}^D \quad M_{12}] \quad \text{and} \\ \mathbf{Q}^T &= [Q_{11}^A \quad Q_{11}^B \quad Q_{22}^C \quad Q_{22}^D \quad Q_{12}] . \end{aligned} \quad (35)$$

In addition, by introducing the matrices

$$\mathbf{A}_N = \mathbf{A}_M = \begin{bmatrix} A_I + A_{II} & 0 & 0 & 0 & 0 \\ 0 & A_{III} + A_{IV} & 0 & 0 & 0 \\ 0 & 0 & A_I + A_{IV} & 0 & 0 \\ 0 & 0 & 0 & A_{II} + A_{III} & 0 \\ 0 & 0 & 0 & 0 & A \end{bmatrix} \quad \text{and} \quad (36a)$$

$$\mathbf{A}_Q = \begin{bmatrix} A_I + A_{II} & 0 & 0 & 0 \\ 0 & A_{III} + A_{IV} & 0 & 0 \\ 0 & 0 & A_I + A_{IV} & 0 \\ 0 & 0 & 0 & A_{II} + A_{III} \end{bmatrix} \quad (36b)$$

along with the discretized strain-displacement relationships, the bilinear approximations for the displacements and rotations, and also the discrete parameters for the strains and stresses, the discrete form of the generalized variational principle of Hu-Washizu is given by

$$\begin{aligned} \Pi_{HW} &= \frac{1}{2} \bar{\boldsymbol{\varepsilon}}^T \bar{\mathbf{D}}_E \bar{\boldsymbol{\varepsilon}} + \frac{1}{2} \bar{\boldsymbol{\kappa}}^T \bar{\mathbf{D}}_B \bar{\boldsymbol{\kappa}} + \frac{1}{2} \bar{\boldsymbol{\varepsilon}}^T \bar{\mathbf{D}}_C \bar{\boldsymbol{\kappa}} + \frac{1}{2} \bar{\boldsymbol{\kappa}}^T \bar{\mathbf{D}}_C \bar{\boldsymbol{\varepsilon}} + \frac{1}{2} \bar{\boldsymbol{\gamma}}^T \bar{\mathbf{D}}_S \bar{\boldsymbol{\gamma}} \\ &\quad - \frac{1}{2} (\mathbf{N}^T \mathbf{A}_N \bar{\boldsymbol{\varepsilon}} + \bar{\boldsymbol{\varepsilon}}^T \mathbf{A}_N \mathbf{N}) - \frac{1}{2} (\mathbf{M}^T \mathbf{A}_M \bar{\boldsymbol{\kappa}} + \bar{\boldsymbol{\kappa}}^T \mathbf{A}_M \mathbf{M}) - \frac{1}{2} (\mathbf{Q}^T \mathbf{A}_Q \bar{\boldsymbol{\gamma}} + \bar{\boldsymbol{\gamma}}^T \mathbf{A}_Q \mathbf{Q}) \\ &\quad + \frac{1}{2} (\mathbf{N}^T \mathbf{E} \boldsymbol{\Delta} + \boldsymbol{\Delta}^T \mathbf{E} \mathbf{N}) + \frac{1}{2} (\mathbf{M}^T \mathbf{B} \boldsymbol{\Delta} + \boldsymbol{\Delta}^T \mathbf{B} \mathbf{M}) + \frac{1}{2} (\mathbf{Q}^T \mathbf{G} \boldsymbol{\Delta} + \boldsymbol{\Delta}^T \mathbf{G} \mathbf{Q}) \end{aligned} \quad (37)$$

The Hu-Washizu variational principle establishes that if the variation is taken with respect to nodal displacements and rotations ($\boldsymbol{\Delta}$), strains, and stresses, then all field equations of elasticity and all boundary conditions appear as Euler-Lagrange equations. In particular, the stationary condition for the functional, $\delta \Pi_{HW} = 0$, enforces the following governing discretized field equation

$$\begin{aligned} &\delta \mathbf{N}^T (\mathbf{E} \boldsymbol{\Delta} - \mathbf{A}_N \bar{\boldsymbol{\varepsilon}}) + \delta \mathbf{M}^T (\mathbf{B} \boldsymbol{\Delta} - \mathbf{A}_M \bar{\boldsymbol{\kappa}}) + \delta \mathbf{Q}^T (\mathbf{G} \boldsymbol{\Delta} - \mathbf{A}_Q \bar{\boldsymbol{\gamma}}) \\ &\quad + \delta \bar{\boldsymbol{\varepsilon}}^T (\bar{\mathbf{D}}_E \bar{\boldsymbol{\varepsilon}} + \bar{\mathbf{D}}_C \bar{\boldsymbol{\kappa}} - \mathbf{A}_N \mathbf{N}) + \delta \bar{\boldsymbol{\kappa}}^T (\bar{\mathbf{D}}_B \bar{\boldsymbol{\kappa}} + \bar{\mathbf{D}}_C \bar{\boldsymbol{\varepsilon}} - \mathbf{A}_M \mathbf{M}) + \delta \bar{\boldsymbol{\gamma}}^T (\bar{\mathbf{D}}_S \bar{\boldsymbol{\gamma}} - \mathbf{A}_Q \mathbf{Q}) \\ &\quad + \delta \boldsymbol{\Delta}^T (\mathbf{E}^T \mathbf{N} + \mathbf{B}^T \mathbf{M} + \mathbf{G}^T \mathbf{Q}) - \delta \boldsymbol{\Delta}^T \mathbf{p} = 0 . \end{aligned} \quad (38)$$

(a) Variation of the stress resultants leads to the discrete strain-displacement relationships

$$\begin{aligned} \mathbf{E} \boldsymbol{\Delta} - \mathbf{A}_N \bar{\boldsymbol{\varepsilon}} = 0 &\implies \bar{\boldsymbol{\varepsilon}} = \mathbf{A}_N^{-1} \mathbf{E} \boldsymbol{\Delta} , \\ \mathbf{B} \boldsymbol{\Delta} - \mathbf{A}_M \bar{\boldsymbol{\kappa}} = 0 &\implies \bar{\boldsymbol{\kappa}} = \mathbf{A}_M^{-1} \mathbf{B} \boldsymbol{\Delta} \quad \text{and} \\ \mathbf{G} \boldsymbol{\Delta} - \mathbf{A}_Q \bar{\boldsymbol{\gamma}} = 0 &\implies \bar{\boldsymbol{\gamma}} = \mathbf{A}_Q^{-1} \mathbf{G} \boldsymbol{\Delta} . \end{aligned} \quad (39)$$

(b) Variation of the strain parameters yields the discrete constitutive equations

$$\begin{aligned} \bar{\mathbf{D}}_E \bar{\boldsymbol{\varepsilon}} + \bar{\mathbf{D}}_C \bar{\boldsymbol{\kappa}} - \mathbf{A}_N \mathbf{N} = 0 &\implies \mathbf{N} = \mathbf{A}_N^{-1} \bar{\mathbf{D}}_E \bar{\boldsymbol{\varepsilon}} + \mathbf{A}_N^{-1} \bar{\mathbf{D}}_C \bar{\boldsymbol{\kappa}} \\ \bar{\mathbf{D}}_B \bar{\boldsymbol{\kappa}} + \bar{\mathbf{D}}_C \bar{\boldsymbol{\varepsilon}} - \mathbf{A}_M \mathbf{M} = 0 &\implies \mathbf{M} = \mathbf{A}_M^{-1} \bar{\mathbf{D}}_B \bar{\boldsymbol{\kappa}} + \mathbf{A}_M^{-1} \bar{\mathbf{D}}_C \bar{\boldsymbol{\varepsilon}} \\ \bar{\mathbf{D}}_S \bar{\boldsymbol{\gamma}} - \mathbf{A}_Q \mathbf{Q} = 0 &\implies \mathbf{Q} = \mathbf{A}_Q^{-1} \bar{\mathbf{D}}_S \bar{\boldsymbol{\gamma}} \end{aligned} \quad (40)$$

(c) Variation of the nodal displacements/rotations leads to the discrete form of the equilibrium equations

$$\mathbf{E}^T \mathbf{N} + \mathbf{B}^T \mathbf{M} + \mathbf{G}^T \mathbf{Q} - \mathbf{p} = 0. \quad (41)$$

By introducing Eqs. (39) in Eqs. (40), the parameters for the stress resultants can be expressed in terms of nodal displacements as

$$\begin{aligned} \mathbf{N} &= \mathbf{A}_N^{-1} \bar{\mathbf{D}}_E \mathbf{A}_N^{-1} \mathbf{E} \Delta + \mathbf{A}_N^{-1} \bar{\mathbf{D}}_C \mathbf{A}_M^{-1} \mathbf{B} \Delta, \\ \mathbf{M} &= \mathbf{A}_M^{-1} \bar{\mathbf{D}}_F \mathbf{A}_M^{-1} \mathbf{B} \Delta + \mathbf{A}_M^{-1} \bar{\mathbf{D}}_C \mathbf{A}_N^{-1} \mathbf{E} \Delta \\ \mathbf{Q} &= \mathbf{A}_Q^{-1} \bar{\mathbf{D}}_S \mathbf{A}_Q^{-1} \mathbf{G} \Delta. \end{aligned} \quad (42)$$

In a compact way, the introduction of expressions (42) into Eq. (41) yields the discrete equilibrium expressed in terms of nodal displacements and rotations as

$$\left[\mathbf{K}_{Extension} + \mathbf{K}_{Bending} + \mathbf{K}_{Coupling} + \mathbf{K}_{Shear} \right] \Delta = \mathbf{p} \quad (43)$$

Therefore, the stiffness matrix, $\mathbf{K}_{20 \times 20}$, is defined by the sum of the following four terms

$$\mathbf{K}_{Extension} = \mathbf{A}_N^{-1} \bar{\mathbf{D}}_E \mathbf{A}_N^{-1} \mathbf{E}, \quad (44)$$

$$\mathbf{K}_{Bending} = \mathbf{B}^T \mathbf{A}_M^{-1} \bar{\mathbf{D}}_F \mathbf{A}_M^{-1} \mathbf{B}, \quad (45)$$

$$\mathbf{K}_{Coupling} = \mathbf{B}^T \mathbf{A}_M^{-1} \bar{\mathbf{D}}_C \mathbf{A}_N^{-1} \mathbf{E} + \mathbf{E}^T \mathbf{A}_N^{-1} \bar{\mathbf{D}}_C \mathbf{A}_M^{-1} \mathbf{B}, \quad (46)$$

$$\mathbf{K}_{Shear} = \mathbf{G}^T \mathbf{A}_Q^{-1} \bar{\mathbf{D}}_S \mathbf{A}_Q^{-1} \mathbf{G}. \quad (47)$$

3.5. The governing eigenvalue equation

The eigenvalue problem for the undamped free vibration problem takes the well-known form

$$\mathbf{K} \mathbf{u} = \omega^2 \mathbf{M} \mathbf{u}, \quad (48)$$

where \mathbf{K} is the stiffness matrix of the system, \mathbf{u} represents the eigenvectors, ω is the natural frequency in rad/s and \mathbf{M} is the mass matrix of the structure. The consistent element mass matrix is derived by discretizing the kinetic energy

$$\delta \mathcal{U}_K = \frac{1}{2} \int_V \rho \mathbf{2} \mathbf{v} \delta \mathbf{v} dV, \quad (49)$$

and by employing the displacement field defined by first-order shear deformation, the integral (49) assumes the form

$$\delta \mathcal{U}_K = \int_A \rho \begin{bmatrix} \delta \ddot{u}_1 & \delta \ddot{u}_2 & \delta \ddot{u}_3 & \delta \ddot{\varphi}_1 & \delta \ddot{\varphi}_2 \end{bmatrix} \begin{bmatrix} I_1 & I_1 \mathcal{A} & 0 & I_2 & I_2 \mathcal{A} \\ I_1 \mathcal{A} & I_1 & 0 & I_2 \mathcal{A} & I_2 \\ 0 & 0 & I_1 & 0 & 0 \\ I_2 & I_2 \mathcal{A} & 0 & I_3 & I_3 \mathcal{A} \\ I_2 \mathcal{A} & I_2 & 0 & I_3 \mathcal{A} & I_3 \end{bmatrix} \begin{bmatrix} u_1 \\ u_2 \\ u_3 \\ \varphi_1 \\ \varphi_2 \end{bmatrix} dA, \quad (50)$$

where the terms I_1, I_2, I_3 and \mathcal{A} (the contravariant components relationship) are defined by

$$I_1 = \int_{-h/2}^{h/2} \rho(z) dz, \quad I_2 = \int_{-h/2}^{h/2} \rho(z) z dz, \quad I_3 = \int_{-h/2}^{h/2} \rho(z) z^2 dz \quad (51)$$

$$\mathcal{A} = \frac{a^{12}}{\sqrt{a^{11} \cdot a^{22}}} = -\cos(\alpha) \quad (52)$$

In addition, by the definition of the displacements and rotations through the shape functions, nodal displacements and nodal rotations in Eq. (25), the consistent mass matrix can be represented by

$$\mathbf{M} = \begin{bmatrix} \mathbf{M}_{11} & \mathbf{M}_{12} & \mathbf{M}_{13} & \mathbf{M}_{14} \\ & \mathbf{M}_{22} & \mathbf{M}_{23} & \mathbf{M}_{24} \\ & & \mathbf{M}_{33} & \mathbf{M}_{34} \\ \text{sym} & & & \mathbf{M}_{44} \end{bmatrix}_{20 \times 20} \quad (53)$$

Every \mathbf{M}_{ij} term of the mass matrix, where i and j represent the row and the column respectively, assumes the following form

$$\mathbf{M}_{ij} = \begin{bmatrix} \int_A I_1 N_i N_j dA & \int_A \mathcal{A} I_1 N_i N_j dA & 0 & \int_A I_2 N_i N_j dA & \int_A \mathcal{A} I_2 N_i N_j dA \\ & \int_A I_1 N_i N_j dA & 0 & \int_A \mathcal{A} I_2 N_i N_j dA & \int_A I_2 N_i N_j dA \\ & & \int_A I_1 N_i N_j dA & 0 & 0 \\ & sym & & \int_A I_3 N_i N_j dA & \int_A \mathcal{A} I_3 N_i N_j dA \\ & & & \int_A I_3 N_i N_j dA & \int_A \mathcal{A} I_3 N_i N_j dA \end{bmatrix}_{5 \times 5} \quad (54)$$

Finally, we remark that all the aspects of numerical implementation associated with the above expressions are carried out by means of the commercial software package MATHEMATICA [53], which is particularly useful for the treatment of symbolic and algebraic computations.

4. Numerical results

In this section, a set of static and free vibration analyses are presented to demonstrate the applicability of the proposed finite element formulation to FG-CNTRC thin and moderately thick skew plates. Firstly, some results are compared to the limited existing bibliography, for isotropic and FG-CNTRC skew plates. Then, new bending and free vibration analyses are presented to broaden knowledge about mechanical characteristics of FG-CNTRC skew plates by taking into consideration not previously considered aspects such as asymmetric reinforcement distributions and orientation of CNTs.

4.1. Comparison studies

In order to show the validity of the proposed finite element formulation, convergence analyses are carried out in order to check the stability of the solution. Also, the free vibration results obtained by Liew et al. [54] and Zhang et al. [4] for isotropic skew plates are compared to the ones obtained by the proposed method. Then, the free vibration results for FG-CNTRC skew plates presented by Zhang et al. [4] are also verified.

4.1.1. Convergence and comparison of free vibration analysis of isotropic skew plates

In these first tests, comparison studies of free vibration analysis are carried out for isotropic skew plates with skew angles $\alpha = 90^\circ, 60^\circ, 45^\circ$ and 30° , thickness-to-width ratios of $t/b = 0.001$ (thin plate) and 0.2 (moderately thick plate) and with four different kinds of boundary conditions, namely all edges simply supported (SSSS) or clamped (CCCC), and two opposite edges simply supported and the other two clamped (SCSC) or free (SFSF). The boundary conditions at any edge can be defined as follows

$$\begin{cases} u_s = u_z = \gamma_s = 0 \Leftarrow \text{Simply supported edge (S)} \\ u_n = u_s = u_z = \gamma_n = \gamma_s = 0 \Leftarrow \text{Clamped edge (C)} \end{cases} \quad (55)$$

where the subscripts n and s denote the normal and tangential directions, respectively. The non-dimensional frequency parameter for vibration analysis is defined by

$$\bar{\omega} = \omega \frac{b^2}{\pi^2} \sqrt{\frac{\rho t}{D}} \quad (56)$$

where ω is the angular frequency of the CNTRC plates, ρ is the plate density per unit volume and $D = Et^3/12(1 - \nu^2)$ is the plate flexural rigidity. A value of $\nu = 0.3$ for Poisson's ratio is used for this analysis. Skew plates are characterized by the presence of stress singularities at the shell corners. Because of the simplifying assumptions commonly adopted, these problems worsen with increasing skew angle and can lead to divergent solutions. Fig. 5 shows the Von Mises stress field of fully clamped isotropic skew plates with increasing skew angles. The existence of stress concentrations at obtuse corners is highlighted. The effect of presence of these singularities on the dynamic characteristics of skew plates is well documented. For example McGee et al. [42] and Huang et al. [55] analyzed the influence of the bending stress singularities by using the Ritz method. By the implementation of comparison functions or so called corner functions the authors studied different boundary conditions and achieved great improvements in the convergence of the solution. The presence of these singularities requires the development of a convergence analysis of the dynamic characteristics in order to prove the stability of the solution. In Fig. 6, the solutions in terms of the first frequency parameter $\bar{\omega}_1$ are represented for four sets of mesh sizes (8×8 , 16×16 , 32×32 and 40×40) and for a skew plate with $a/b = 1$, $\alpha = 45^\circ$ and $t/b = 0.2$ having CCCC and SFSF boundary conditions. As expected, fewer elements are needed for the lower modes to reach an acceptable convergence as compared to the higher modes. These studies show that 24×24 elements are sufficient to reach accurate vibration results. Therefore, for the subsequent calculations, this mesh size is adopted.

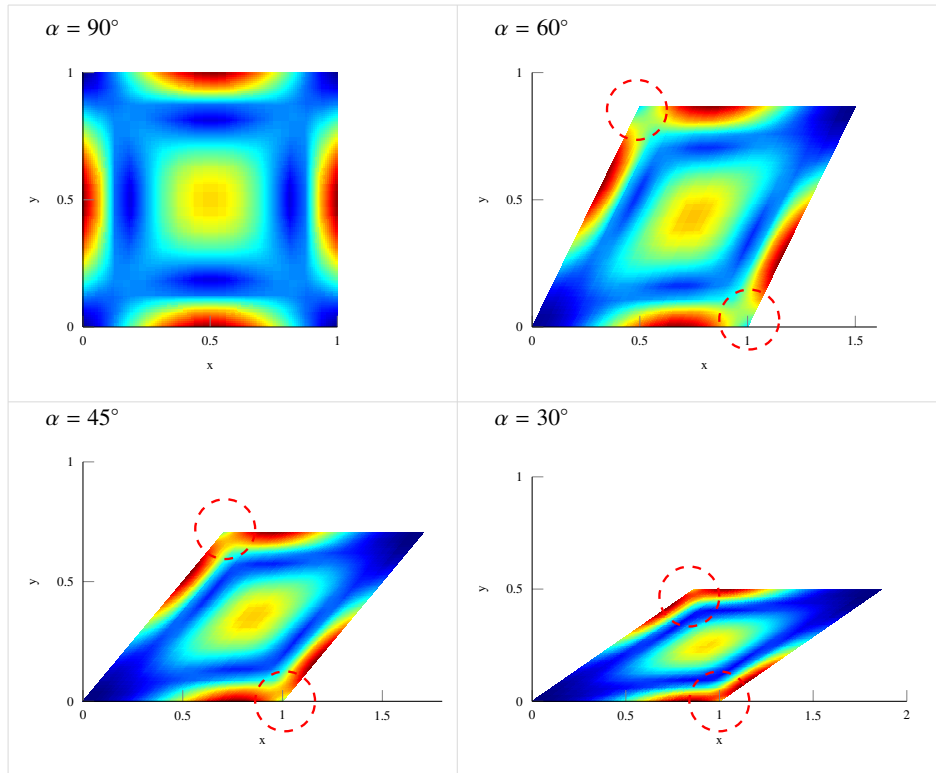


Figure 5: Corner stress singularities (Von Mises) of fully clamped (CCCC) isotropic skew plates subjected to transverse uniform loading ($q_o = -0.1\text{MPa}$) and varying skew angle ($\alpha = 90^\circ, 60^\circ, 45^\circ$ and 30°)

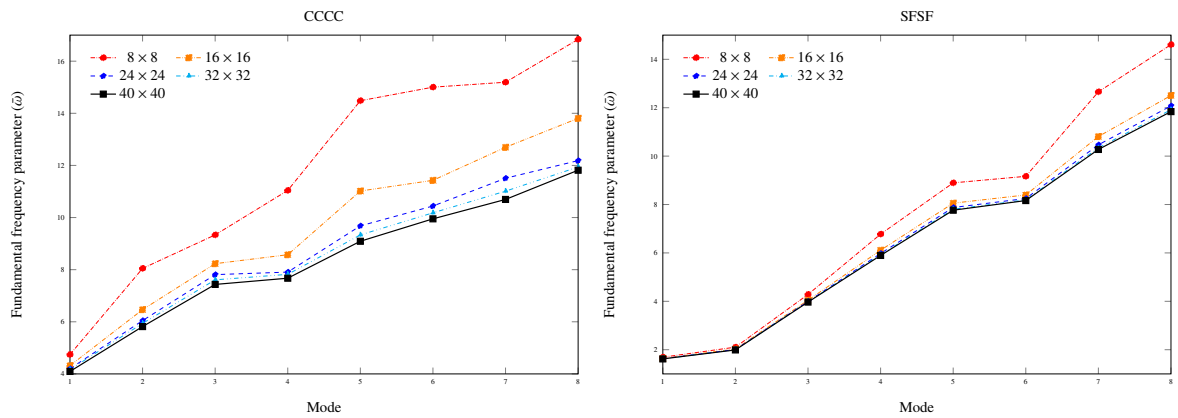


Figure 6: First frequency parameter $\bar{\omega}_1$ convergence analysis for SSSS and SFSF isotropic skew plates in terms of mesh size $N \times N$ ($a/b = 1$, $t/b = 0.2$, $\alpha = 45^\circ$, $\varphi = 0^\circ$)

Table 1: Comparison study of frequency parameters $(\omega^2/\pi^2)/\sqrt{\rho t/D}$ of isotropic skew plates with CCCC boundary conditions ($a/b = 1$, $t/b=0.001$, $\varphi = 0^\circ$).

t/b	Modes	Skew Angle α											
		90°			75°			60°			45°		
		Present	Ref. [4]	Ref. [54]	Present	Ref. [4]	Ref. [54]	Present	Ref. [4]	Ref. [54]	Present	Ref. [4]	Ref. [54]
0.001	1	3.6512	3.6021	3.6360	3.8886	3.8643	3.8691	4.6989	4.6216	4.6698	6.7154	6.5723	6.6519
	2	7.4739	7.3583	7.4362	7.5021	7.3733	7.3858	8.4284	8.1379	8.2677	11.0973	10.6458	10.7898
	3	7.4739	7.3955	7.4362	8.4876	8.3593	8.3708	10.8167	10.6482	10.6554	15.6810	14.8760	15.0276
	4	11.0081	10.9244	10.9644	11.2957	11.1428	11.1005	12.4007	11.9301	12.0825	16.2328	15.9282	15.9342
	5	13.4939	13.2120	13.3317	14.5552	14.1079	14.0806	17.3787	16.5326	16.7159	21.2248	19.7857	19.9365
	6	13.5591	13.3697	13.3948	15.1431	14.7384	14.7064	17.3915	16.5452	16.7496	24.4016	23.0641	23.2526
	7	16.8548	16.6561	16.7174	16.4287	16.0198	15.9652	19.4045	18.9924	18.8644	27.2306	25.0774	25.1799
	8	16.8548	16.7767	16.7174	19.1739	18.6578	18.6397	23.1179	21.9124	22.1064	30.2685	29.2970	29.2107
0.2	1	2.6912	2.6616	2.6807	2.8173	2.8131	2.8058	3.2466	3.2220	3.2313	4.1853	4.0947	4.1590
	2	4.7156	4.6459	4.6753	4.6739	4.6535	4.6298	5.0324	4.9674	4.9757	5.9945	5.8162	5.9021
	3	4.7156	4.6636	4.6753	5.1384	5.1299	5.0963	6.0647	6.0128	6.0139	7.7144	7.4336	7.5422
	4	6.3248	6.2438	6.2761	6.3715	6.3372	6.3070	6.7188	6.6142	6.6217	7.8656	7.6724	7.7907
	5	7.2650	7.1329	7.1496	7.5282	7.4828	7.4052	8.4143	8.2749	8.2634	9.5148	9.0902	9.2159
	6	7.3664	7.2384	7.2482	7.8313	7.6600	7.7179	8.5304	8.3584	8.3595	10.3179	9.9502	10.0921
	7	8.5867	8.4610	8.4822	8.3138	8.2415	8.1914	9.1975	9.0923	9.0729	11.2759	10.6947	10.8388
	8	8.5867	8.4613	8.4822	9.2214	9.1741	9.0900	10.2954	10.1002	10.0837	12.0633	11.8158	11.8618

Table 2: Material properties of Poly (methyl methacrylate)(PMMA) at room temperature of 300K and (10, 10) single walled carbon nanotubes (SWCNT).

(10, 10) SWCNT [16]	PMMA (T = 300K)
$E_{11}^{CNT} = 5.6466TPa$	$E^m = 2.5GPa$
$E_{22}^{CNT} = 7.0800TPa$	$\nu^m = 0.34$
$G_{12}^{CNT} = 1.9445TPa$	$\alpha^m = 45 \times 10^{-6}/K$
$\nu_{12}^{CNT} = 0.175$	

The first eight frequency parameters for CCCC boundary conditions are presented in Table 1 together with the published results in references [54] and [4]. It can be seen that the present frequency parameters match very well for all cases. It is remarkable that the stiffening effect of increasing skew angles in this type of structural element is seen in all posterior results.

4.1.2. Convergence and comparison of free vibration analysis of FG-CNTRC skew plates

The next comparison analysis refers to free vibration of FG-CNTRC skew plates. A new convergence analysis is performed in order to check the suitability of the discretization for accurate predictions of this new scenario with transversely isotropic materials. The matrix Poly (methyl methacrylate), referred to as PMMA, is selected and the material properties are assumed to be $\nu^m = 0.34$, $\alpha^m = 45 \cdot (1 + 0.0005 \cdot \Delta t) \times 10^{-6}/K$ and $E^m = (3.52 - 0.0034 \cdot T)GPa$. The armchair (10,10) SWCNTs are selected as reinforcements with properties taken from the MD simulation carried out by Shen and Zhang [16]. The material properties of these two phases are summarized in Table 2. In this study, it is assumed that the effective material properties are independent of the geometry of the CNTRC plates. The detailed material properties of PMMA/CNT for the FG-CNTRC skew plates are selected from the MD results reported by Han and Elliot [56]. The CNT efficiency parameters are taken from [16] and are presented in Table 3.

In this section, the nondimensional frequency parameter $\bar{\omega}$ is defined for composites by using the matrix's material properties as follows

$$\bar{\omega} = \omega \frac{b^2}{\pi^2} \sqrt{\frac{\rho^m t}{D}}; \quad D = E^m t^3 / 12(1 - \nu^m) \quad (57)$$

In Fig. 7, the solutions in terms of the first frequency parameter $\bar{\omega}_1$ for the mesh sizes $(8 \times 8, 16 \times 16, 32 \times 32$

Table 3: Comparison of Young's moduli for PMMA/CNT composites reinforced by (10, 10) SWCNT at T=300K with MD simulation [16]

V_{CNT}^*	MD [16]			Rule of mixtures		
	$E_{11}(GPa)$	$E_{22}(GPa)$	$\bar{E}_{11}(GPa)$	η_1	$E_{22}(GPa)$	η_2
0.12	94.6	2.9	94.8	0.137	2.9	1.022
0.17	138.2	4.9	138.7	0.142	4.9	1.626
0.28	224.2	5.5	224.0	0.141	5.5	1.585

Table 4: Comparison study of frequency parameters $\bar{\omega}$ for a skew plate with CCCC boundary conditions ($a/b = 1$, $t/b=0.001$, $\varphi = 0^\circ$)

Skew angle α	Mode	UD						FG-X					
		0.12		0.17		0.28		0.12		0.17		0.28	
		Present	Ref [4]	Present	Ref [4]	Present	Ref [4]	Present	Ref [4]	Present	Ref [4]	Present	Ref [4]
90°	1	13.304	13.054	16.027	15.792	20.017	19.745	16.110	15.875	19.429	19.155	24.390	24.059
	2	14.803	14.382	18.087	17.714	21.848	21.472	17.455	17.026	21.352	20.810	26.313	25.703
	3	18.686	17.853	23.327	22.600	26.734	26.017	21.077	20.307	26.432	25.419	31.547	30.443
	4	25.623	23.172	32.514	31.432	35.729	34.652	27.829	26.627	35.680	34.078	41.388	39.656
	5	35.762	31.900	43.722	41.809	49.142	45.057	37.991	35.095	49.364	45.527	56.287	52.073
	6	36.386	35.743	44.862	43.768	54.927	47.702	44.258	36.474	53.251	47.365	67.053	54.094
60°	1	13.741	13.447	16.625	16.264	20.550	20.160	16.503	16.192	19.988	19.602	24.949	24.505
	2	16.351	15.672	20.164	19.278	23.809	22.934	18.912	18.243	23.386	22.489	28.421	27.454
	3	22.205	20.498	27.931	25.693	31.369	29.132	24.577	22.875	31.171	28.871	36.665	34.168
	4	31.566	28.091	40.080	35.593	43.849	39.190	34.055	30.497	43.871	39.135	50.572	45.335
	5	37.045	36.444	44.638	43.923	55.712	52.351	44.835	40.615	54.080	52.372	67.861	60.275
	6	38.772	37.350	47.029	45.782	57.732	54.907	46.156	44.179	56.256	53.301	69.228	66.933
45°	1	14.901	14.395	18.194	17.559	21.999	21.321	17.577	17.041	21.498	20.817	26.492	25.710
	2	19.853	18.648	24.770	23.211	28.389	26.801	22.362	21.148	28.080	26.466	33.455	31.689
	3	29.062	26.713	36.695	33.674	40.720	37.565	31.745	29.319	40.609	37.395	47.238	43.658
	4	38.750	37.401	47.034	45.698	57.205	53.004	44.955	41.263	56.077	52.803	66.944	61.342
	5	41.578	38.448	52.318	48.114	58.827	56.759	46.743	45.500	58.302	55.338	70.466	68.774
	6	43.160	41.690	53.022	51.110	63.210	61.322	50.347	48.869	61.946	60.005	75.748	73.589
30°	1	19.519	18.708	24.306	23.390	27.984	27.144	22.076	21.312	27.650	26.607	33.038	31.948
	2	30.336	28.584	38.184	36.180	42.701	40.691	33.351	31.586	42.511	40.162	49.680	47.110
	3	44.851	41.961	56.232	53.285	63.394	60.238	49.561	46.447	63.029	59.042	73.849	69.254
	4	47.506	46.437	58.847	58.026	68.706	68.432	54.450	53.656	67.642	66.426	81.652	80.601
	5	61.500	57.751	76.983	73.156	87.185	83.244	68.285	64.292	86.573	81.438	101.831	95.940
	6	62.117	57.990	78.307	74.953	87.462	84.869	68.430	65.105	87.017	81.967	102.007	97.367

and 40×40) are represented for a skew plate with $a/b = 1$, $\alpha = 30^\circ$, UD-CNTRC, $V_{CNT}^* = 0.12$ and $t/b = 0.001$ having CCCC and SFSF boundary conditions. As in the previous case, a mesh pattern of 24×24 is considered sufficient for convergence, and, henceforth this mesh size is adopted.

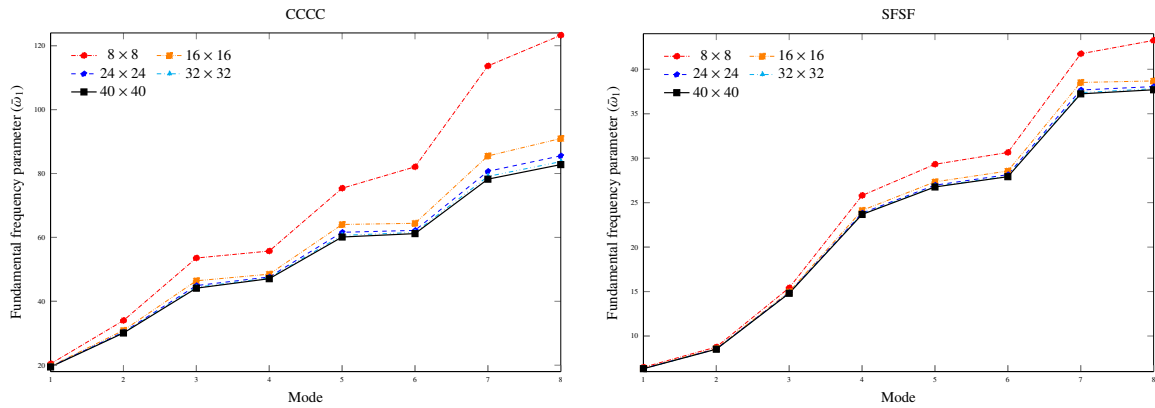


Figure 7: First frequency parameter $\bar{\omega}_1$ convergence analysis for SSSS and SFSF FG-CNTRC skew plates in terms of mesh size $N \times N$ (UD-CNTRC, $V_{CNT}^* = 0.12$, $a/b = 1$, $t/b = 0.001$, $\alpha = 30^\circ$, $\varphi = 0^\circ$)

The results obtained by Zhang et al. [4] are compared to the ones obtained by the proposed method. Comparison of the first eight frequency parameters of the fully clamped CNTRC skew plates with uniform and FG-X distributions of reinforcement is given in Table 4. As previously noted, decreasing skew angles result in higher natural frequencies. Moreover, results provided by Zhang et al. [4] about the influence of the aspect ratio t/b on the non-dimensional frequency parameter are also compared with the proposed approach in Table 5. Here it is also noticeable that increasing the a/b ratio decreases the frequency parameters. It can be seen that the results obtained by the proposed methodology match very well with the cited reference in both analyses. These close agreements, in combination with the convergence analyses, serve to verify the present approach and establish the foundation for its application to FG-CNTRC skew plates.

4.2. Results for FG-CNTRC skew plates

The results obtained by the proposed methodology have been shown to be stable and similar to those provided in the literature. Some new results are now presented. Here we analyze the static response of functionally graded

Table 5: Comparison study of frequency parameters $\bar{\omega}$ of uniform CNTRC skew plates of various aspect ratios with CCCC boundary conditions (UD-CNTRC, $V_{CNT}=0.12$, $t/b = 0.001$, $\varphi = 0^\circ$)

Skew angle α	Mode	Frequency parameters $\bar{\omega}$									
		$a/b = 1$		$a/b = 1.5$		$a/b = 2$		$a/b = 2.5$		$a/b = 3$	
		Present	Ref [4]	Present	Ref [4]	Present	Ref [4]	Present	Ref [4]	Present	Ref [4]
90°	1	13.304	13.054	6.308	6.087	4.055	3.863	3.156	2.959	2.755	2.546
	2	14.803	14.382	8.836	8.258	7.304	6.698	6.349	6.151	4.740	4.568
	3	18.686	17.853	14.212	12.940	9.461	9.193	6.799	6.169	6.596	5.946
	4	25.623	23.172	16.377	15.918	11.458	10.959	8.927	8.430	7.781	7.257
	5	35.762	31.900	17.749	17.135	13.231	11.911	11.872	11.482	8.449	8.215
	6	36.386	35.743	21.272	20.071	16.144	15.046	12.920	11.622	10.624	10.237
60°	1	13.741	13.447	6.792	6.572	4.626	4.379	3.800	3.491	3.445	3.108
	2	16.351	15.672	10.636	9.774	9.051	8.219	6.766	6.563	5.245	5.059
	3	22.205	20.498	16.891	15.508	10.148	9.870	8.909	7.927	8.670	7.652
	4	31.566	28.091	17.424	16.602	12.901	12.126	10.521	9.763	8.697	8.317
	5	37.045	36.444	19.988	18.964	17.467	15.232	12.482	12.359	9.905	9.373
	6	38.772	37.350	23.960	21.826	18.827	17.214	14.747	13.946	12.015	11.405
45°	1	14.901	14.395	7.958	7.498	5.910	5.371	5.183	4.572	4.888	4.243
	2	19.853	18.648	14.148	13.038	10.651	10.109	7.848	7.398	6.426	5.953
	3	29.062	26.713	18.458	17.781	13.697	12.579	12.588	11.848	9.688	9.239
	4	38.750	37.401	21.270	19.860	15.932	14.820	13.094	11.850	12.890	11.718
	5	41.578	38.448	27.367	25.013	20.423	19.632	15.258	14.315	13.893	12.811
	6	43.160	41.690	29.641	27.684	22.403	20.928	17.455	16.268	14.161	13.347
30°	1	19.519	18.833	12.075	10.989	10.173	8.691	9.589	8.003	9.370	7.534
	2	30.336	28.794	20.737	19.250	14.488	13.234	11.737	10.314	10.523	8.858
	3	44.851	42.532	28.489	25.438	21.919	20.353	16.375	15.059	13.319	11.873
	4	47.506	47.009	30.212	27.993	26.186	22.302	22.906	21.030	17.920	16.283
	5	61.500	58.532	41.575	38.641	30.297	27.013	25.826	21.843	23.805	21.490
	6	62.117	59.749	42.194	39.345	30.299	27.868	27.220	23.377	25.614	22.642

PMMA/CNT skew plates under uniform transverse loads (q_o), the free vibration analysis of FG skew plates with symmetrical and unsymmetrical reinforcement distributions, and finally we show the advantages of the invariant definition of the constitutive relationships from the analysis of the influence of fiber direction on the natural frequencies. The various non-dimensional parameters used within this section are defined as

$$\text{Non-dimensional frequency parameter} : \lambda = \omega \frac{b^2}{t} \sqrt{\frac{\rho^m}{E^m}}, \quad (58a)$$

$$\text{Central deflection} : \bar{w} = \frac{u_z}{t} \quad (58b)$$

$$\text{Central axial stress} : \bar{\sigma} = \frac{\sigma \cdot t^2}{|q_o| \cdot a^2} \quad (58c)$$

where w_o is the vertical deflection at the central point. Note the non-dimensional frequency parameter is slightly different from the one employed earlier.

4.2.1. Bending of FG-CNTRC skew plates

Several numerical examples are provided to investigate the bending analysis of FG-CNTRC skew plates under uniform transverse loading $q_o = -0.1 \text{MPa}$. Four types of FG skew plates, UD-CNTRC, FG-V, FG-O and FG-X CNTRC are considered with several boundary conditions. In order to demonstrate the accuracy of the FE model used in the present study, results given by ANSYS (SHELL181, four-noded element with six degrees of freedom at each node) for the same mesh density are provided. Tables 6 and 7 shows the non-dimensional central deflection \bar{w} for the four types of FG CNTRC skew plates subjected to a uniform transverse load q_o with different values of width-to-thickness ratio ($b/t=10, 50$) and varying skew angles for SSSS and CCCC boundary conditions. It is noticeable that the volume fraction of the CNTs has so much influence on the central deflection of the plates. For instance, for uniform distributions only 6% increase in the volume fraction of CNT may lead to more than 60% decrease in the central deflection. Likewise, the values of non-dimensional deflections decrease as the skew angle increases. It is also notable that the central deflections of FG-V and FG-O CNTRC plates are larger than the deflections of UD-CNTRC plates while those of the FG-X CNTRC plates are smaller. This is because the profile

Table 6: Effects of CNT volume fraction V_{CNT} and width-to-thickness ratio (b/t) on the non-dimensional central deflection w_o/t for CNTRC skew plates under a uniformly distributed load $q_0 = -0.1\text{MPa}$ with SSSS boundary conditions ($a/b=1, \varphi = 0^\circ$).

V_{CNT}	b/t	α	UD		FG - X		FG - V		FG - O		
			Present	ANSYS	Present	ANSYS	Present	ANSYS	Present	ANSYS	
0.12	10	90	2.831E-03	2.828E-03	2.274E-03	2.271E-03	2.983E-03	2.980E-03	4.341E-03	4.337E-03	
		60	2.698E-03	2.558E-03	2.245E-03	2.094E-03	2.812E-03	2.678E-03	3.824E-03	3.719E-03	
		45	2.210E-03	2.038E-03	1.913E-03	1.721E-03	2.279E-03	2.117E-03	2.856E-03	2.741E-03	
		30	1.181E-03	1.115E-03	1.073E-03	9.917E-04	1.200E-03	1.141E-03	1.364E-03	1.335E-03	
	50	90	1.134E+00	1.133E+00	7.736E-01	7.733E-01	1.232E+00	1.232E+00	2.105E+00	2.105E+00	
		60	1.045E+00	1.040E+00	7.376E-01	7.329E-01	1.125E+00	1.120E+00	1.797E+00	1.794E+00	
		45	8.319E-01	8.261E-01	6.202E-01	6.135E-01	8.890E-01	8.824E-01	1.282E+00	1.278E+00	
		30	4.300E-01	4.267E-01	3.489E-01	3.443E-01	4.586E-01	4.528E-01	5.721E-01	5.719E-01	
	0.17	10	90	1.836E-03	1.834E-03	1.450E-03	1.448E-03	1.935E-03	1.933E-03	2.866E-03	2.863E-03
			60	1.720E-03	1.641E-03	1.404E-03	1.320E-03	1.789E-03	1.715E-03	2.480E-03	2.423E-03
			45	1.380E-03	1.286E-03	1.169E-03	1.065E-03	1.417E-03	1.331E-03	1.813E-03	1.752E-03
			30	7.186E-04	6.847E-04	6.361E-04	5.956E-04	7.248E-04	6.960E-04	8.440E-04	8.308E-04
50		90	7.732E-01	7.731E-01	5.277E-01	5.275E-01	8.404E-01	8.403E-01	1.436E+00	1.436E+00	
		60	7.008E-01	6.984E-01	4.940E-01	4.914E-01	7.533E-01	7.509E-01	1.204E+00	1.202E+00	
		45	5.440E-01	5.408E-01	4.031E-01	3.995E-01	5.796E-01	5.758E-01	8.390E-01	8.370E-01	
		30	2.710E-01	2.694E-01	2.162E-01	2.139E-01	2.873E-01	2.838E-01	3.639E-01	3.642E-01	
0.28		10	90	1.320E-03	1.318E-03	1.047E-03	1.045E-03	1.359E-03	1.357E-03	1.988E-03	1.986E-03
			60	1.291E-03	1.210E-03	1.041E-03	9.641E-04	1.305E-03	1.233E-03	1.820E-03	1.756E-03
			45	1.089E-03	9.878E-04	8.901E-04	7.941E-04	1.080E-03	9.916E-04	1.425E-03	1.349E-03
			30	6.040E-04	5.611E-04	4.992E-04	4.600E-04	5.824E-04	5.487E-04	7.218E-04	6.945E-04
	50	90	4.841E-01	4.839E-01	3.281E-01	3.280E-01	5.278E-01	5.276E-01	9.280E-01	9.279E-01	
		60	4.570E-01	4.546E-01	3.150E-01	3.126E-01	4.905E-01	4.883E-01	8.245E-01	8.226E-01	
		45	3.780E-01	3.746E-01	2.676E-01	2.641E-01	3.980E-01	3.947E-01	6.212E-01	6.188E-01	
		30	2.069E-01	2.046E-01	1.530E-01	1.506E-01	2.134E-01	2.106E-01	2.965E-01	2.957E-01	

of the reinforcement distribution affects the stiffness of the plates. This phenomenon highlights the advantage of FG materials, in which a desired stiffness can be achieved by adjusting the distribution of CNTs along the thickness direction of the plates. It is concluded that reinforcements distributed close to the top and bottom induce higher stiffness values of plates. Figure 8 shows the non-dimensional central deflections of skew plates with $a/b = 1$, $V_{CNT} = 17\%$, $b/t = 50$, for SSSS and CCCC boundary conditions. The stiffening effect of higher values of skew angle α can be seen clearly. Similar conclusions can be extracted from stress analysis. Fig. 9 shows the non-dimensional stress $\bar{\sigma}_{xx}$ distribution along the thickness for CNTRC skew plates with a skew angle of $\alpha = 30^\circ$, subjected to a uniform transverse load q_o with the volume fraction $V_{CNT} = 17\%$. Due to the symmetric distribution (with respect to the mid-plane) of reinforcements for UD, FG-O and FG-X CNTRC skew plates, the central axial stress distributions is anti-symmetric. In the case of FG-V CNTRC and FG-O CNTRC skew plates, the axial stress is close to zero at the bottom and top respectively. This is because the concentration of CNTs vanishes at these points for these two distributions.

4.2.2. Free vibration analysis FG-CNTRC skew plates

The free vibration analyses of fully clamped and simply supported FG-CNTRC skew plates are given in Tables 8 and 9. The presented four types of CNTRC are considered with the CNT volume fractions of 12%, 17% and 28%. The plate geometry is defined by the following parameters, $a/b=1$ and $b/t=10, 50$. Here we present the first free vibration analysis of asymmetric FG-CNTRC skew plates, and the results are compared to those from the commercial code ANSYS. Figure 10 shows the evolution of the frequency parameters with varying skew angles for each reinforcement distribution separately. As expected from the previous analysis, higher skew angles give stiffer behaviors and therefore higher frequency parameters. This can be explained in terms of the plate area and the perpendicular distance between the non-skew edges. With higher skew angles, the distance between the non-skew edges decreases which increases the frequency values. Furthermore, larger volume fractions of CNTs lead to higher values of frequency parameters, due to an increase in the stiffness of the CNTRC plate when the CNT volume fraction is higher. Moreover, as could be seen in the bending simulations, we observe that the FG-X plates lead to the stiffest solutions and possess the highest frequency parameters. The explanation of this phenomenon is the same as mentioned before; reinforcements distributed closer to the extremes result in stiffer plates than those distributed nearer to the mid-plane.

Fig. 11 shows the vibration mode shapes of fully clamped UD-CNTRC plates ($V_{CNT}^* = 12\%$, $a/b = 1$ and

Table 7: Effects of CNT volume fraction V_{CNT} and width-to-thickness ratio (b/t) on the non-dimensional central deflection w_o/t for CNTRC skew plates under a uniformly distributed load $q_0 = -0.1\text{MPa}$ with CCCC boundary conditions ($a/b=1, \varphi = 0^\circ$).

V_{CNT}	b/t	α	UD		FG - X		FG - V		FG - O		
			Present	ANSYS	Present	ANSYS	Present	ANSYS	Present	ANSYS	
0.12	10	90	1.371E-03	1.368E-03	1.263E-03	1.260E-03	1.516E-03	1.513E-03	1.673E-03	1.669E-03	
		60	1.318E-03	1.227E-03	1.227E-03	1.135E-03	1.415E-03	1.336E-03	1.537E-03	1.464E-03	
		45	1.025E-03	9.607E-04	9.628E-04	8.952E-04	1.069E-03	1.022E-03	1.145E-03	1.107E-03	
		30	4.942E-04	5.211E-04	4.701E-04	4.931E-04	5.016E-04	5.357E-04	5.282E-04	5.691E-04	
	50	90	2.406E-01	2.403E-01	1.689E-01	1.687E-01	3.420E-01	3.417E-01	4.470E-01	4.467E-01	
		60	2.389E-01	2.341E-01	1.720E-01	1.671E-01	3.266E-01	3.215E-01	4.164E-01	4.126E-01	
		45	2.119E-01	2.056E-01	1.597E-01	1.527E-01	2.717E-01	2.647E-01	3.335E-01	3.293E-01	
		30	1.248E-01	1.223E-01	1.021E-01	9.861E-02	1.437E-01	1.401E-01	1.662E-01	1.656E-01	
	0.17	10	90	8.443E-04	8.424E-04	7.646E-04	7.628E-04	9.405E-04	9.384E-04	1.050E-03	1.048E-03
			60	8.037E-04	7.522E-04	7.338E-04	6.830E-04	8.656E-04	8.222E-04	9.538E-04	9.130E-04
			45	6.189E-04	5.845E-04	5.686E-04	5.338E-04	6.453E-04	6.218E-04	7.031E-04	6.839E-04
			30	2.956E-04	3.137E-04	2.745E-04	2.909E-04	2.986E-04	3.211E-04	3.205E-04	3.464E-04
50		90	1.635E-01	1.633E-01	1.139E-01	1.137E-01	2.342E-01	2.340E-01	3.063E-01	3.060E-01	
		60	1.602E-01	1.575E-01	1.145E-01	1.117E-01	2.197E-01	2.167E-01	2.809E-01	2.788E-01	
		45	1.389E-01	1.355E-01	1.036E-01	9.985E-02	1.776E-01	1.737E-01	2.197E-01	2.176E-01	
		30	7.862E-02	7.742E-02	6.313E-02	6.148E-02	8.982E-02	8.789E-02	1.058E-01	1.056E-01	
0.28		10	90	6.910E-04	6.893E-04	6.133E-04	6.118E-04	7.297E-04	7.278E-04	8.044E-04	8.028E-04
			60	6.733E-04	6.224E-04	5.920E-04	5.483E-04	6.911E-04	6.480E-04	7.648E-04	7.187E-04
			45	5.298E-04	4.918E-04	4.598E-04	4.299E-04	5.295E-04	5.013E-04	5.911E-04	5.587E-04
			30	2.587E-04	2.705E-04	2.229E-04	2.368E-04	2.516E-04	2.670E-04	2.819E-04	2.959E-04
	50	90	1.038E-01	1.037E-01	7.316E-02	7.310E-02	1.486E-01	1.484E-01	1.938E-01	1.935E-01	
		60	1.050E-01	1.024E-01	7.500E-02	7.249E-02	1.445E-01	1.421E-01	1.866E-01	1.844E-01	
		45	9.626E-02	9.260E-02	7.017E-02	6.659E-02	1.238E-01	1.206E-01	1.577E-01	1.550E-01	
		30	6.011E-02	5.839E-02	4.526E-02	4.347E-02	6.866E-02	6.711E-02	8.566E-02	8.484E-02	

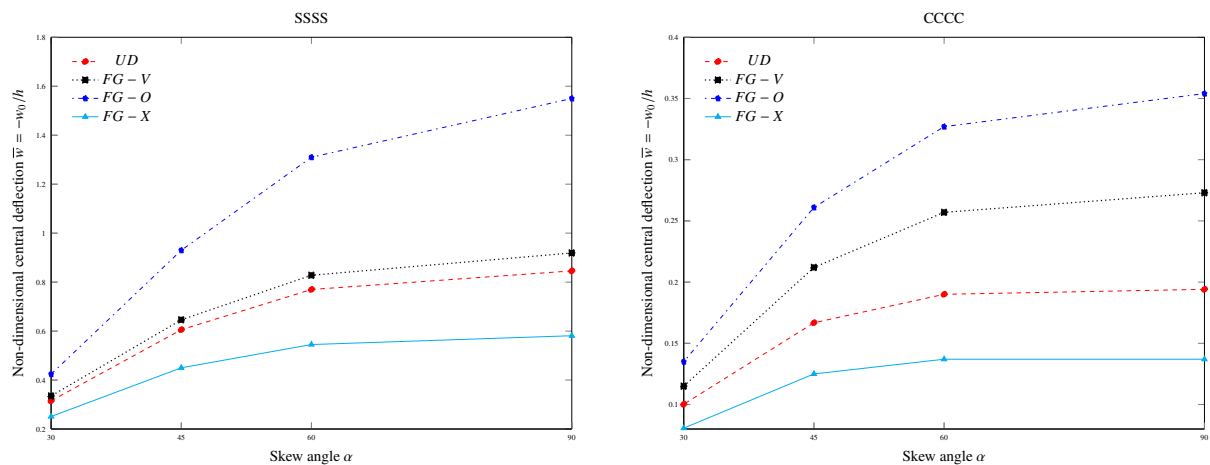


Figure 8: Variation of the non-dimensional central deflection w_o/t under uniformly distributed load $q_0 = -0.1\text{MPa}$ with SSSS and CCCC boundary conditions ($a/b = 1, V_{CNT} = 17\%, b/t = 50, \varphi = 0^\circ$)

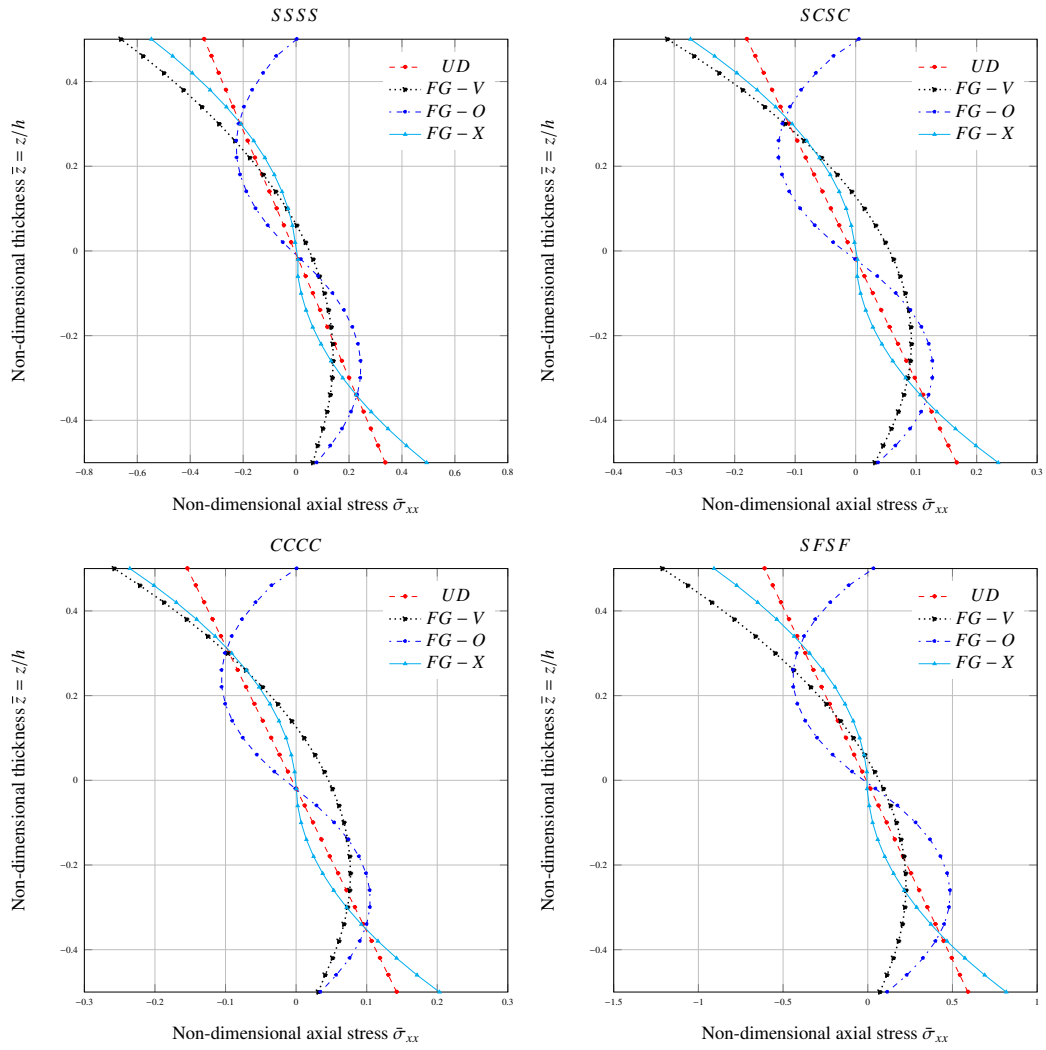


Figure 9: Non-dimensional central axial stress $\bar{\sigma}_{xx} = \frac{\sigma_{xx}}{|q_0|a^2}$ in CNTRC skew plates under a uniform load $q_0 = -0.1\text{MPa}$ and various boundary conditions ($V_{CNT} = 17\%$, $a/b = 1$, $b/t = 50$, $\alpha = 30^\circ$, $\varphi = 0^\circ$)

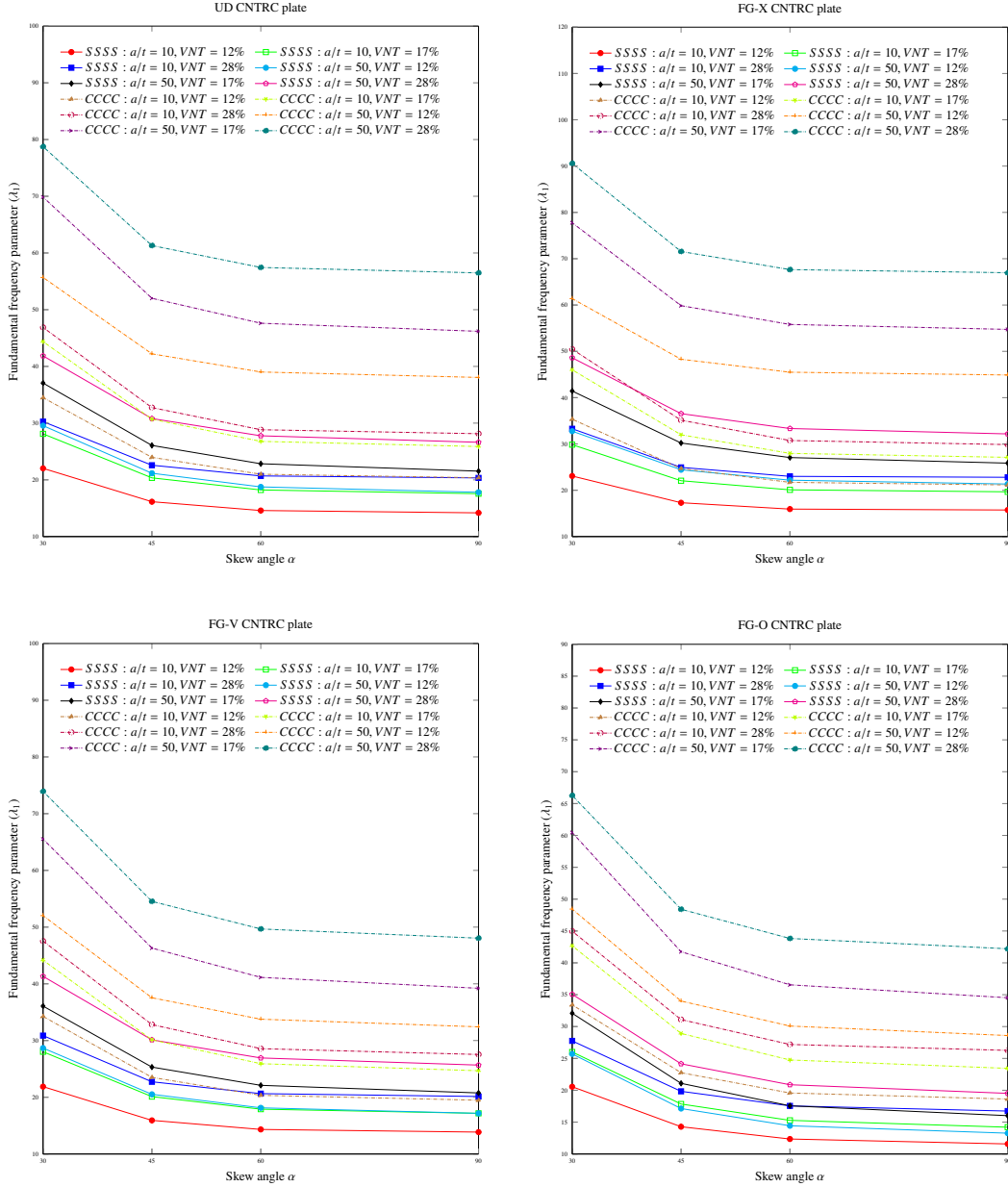


Figure 10: Effect of CNT volume fraction on the first frequency parameter λ_1 ($a/b=1$, $\varphi = 0^\circ$).

$t/b = 0.02$) for skew angles $\alpha = 90^\circ, 60^\circ, 45^\circ$ and 30° . It is observed from these figures that mode crossing occurs as the skew angle increases.

4.2.3. Effect of direction of CNTs in FG-CNTRC skew plates on natural frequencies

Taking advantage of the invariant definition of the constitutive tensor for transversely isotropic materials, characterized by a unit vector parallel to the axis of the transverse isotropy, $\vec{n} = (\cos \varphi, \sin \varphi, 0)$, we analyze the influence of the angle φ on the frequency parameters λ . Figure 12 shows the variation of the first frequency parameter for several values of skew angle α and two boundary conditions, CCCC and SSSS. As in all the previous analyses, the frequency parameters increase for higher values of skew angle. Moreover, the results for skew angles of $\alpha = 90^\circ$ are perfectly symmetric around $\varphi = 90^\circ$. In contrast, the curves for higher skew angles present increasing levels of asymmetry. This is due to the increment of stiffness provided by fibers coupled with the stiffening effect of the skew angle. The curves can be separated into two sets divided around $\varphi = 90^\circ$. For the SSSS boundary condition set, it is clear that the increased stiffness is associated with fibers aligning the direction of the longest diagonal. Otherwise, the frequency values for the second set decreases in all cases for fiber angles above $\varphi = 90^\circ$. In the case of the CCCC boundary condition set this behavior is repeated although the maximum values are approximately obtained with fibers aligned in the horizontal Cartesian direction. This result shows the

Table 8: Comparison study of frequency parameter λ_1 of skew plates with SSSS boundary conditions ($a/b = 1, \varphi = 0^\circ$)

Skew angle	ν_{CNT}	b/t	Mode	Types							
				UD		FG - V		FG - O		FG - X	
				Present	ANSYS	Present	ANSYS	Present	ANSYS	Present	ANSYS
90°	0.12	10	1	14.181	14.254	13.859	13.934	11.576	11.644	15.734	15.810
			2	18.364	18.611	18.185	18.433	16.410	16.642	19.717	19.976
			3	28.090	28.710	28.086	28.707	26.660	27.272	29.345	29.972
		50	1	17.808	17.807	17.167	17.164	13.264	13.263	21.343	21.341
			2	22.378	22.372	21.931	21.913	18.738	18.738	25.525	25.515
			3	34.465	34.485	34.320	34.293	31.696	31.727	37.247	37.259
	0.17	10	1	17.562	17.656	17.168	17.262	14.202	14.287	19.665	19.762
			2	23.181	23.498	23.015	23.331	20.590	20.886	25.163	25.495
			3	35.965	36.763	36.096	36.897	33.905	34.696	38.070	38.877
		50	1	21.536	21.534	20.763	20.765	16.014	16.013	25.858	25.855
			2	27.750	27.744	27.283	27.284	23.260	23.262	31.765	31.755
			3	43.779	43.808	43.792	43.833	40.044	40.086	47.830	47.853
	0.28	10	1	20.343	20.443	20.135	20.239	16.737	16.831	22.798	22.904
			2	25.656	25.998	25.748	26.090	22.491	22.810	28.579	28.944
			3	38.461	39.303	39.124	39.976	35.516	36.364	42.446	43.304
		50	1	26.620	26.617	25.670	25.673	19.515	19.513	32.167	32.164
			2	32.274	32.262	31.779	31.775	25.893	25.889	38.150	38.134
			3	47.900	47.916	48.312	48.345	41.894	41.924	55.183	55.200
60°	0.12	10	1	14.592	15.087	14.327	14.784	12.350	12.617	15.933	16.596
			2	21.101	21.661	20.926	21.465	19.411	19.824	22.313	22.987
			3	32.873	34.092	32.583	33.819	31.282	32.395	34.098	35.414
		50	1	18.756	18.792	18.137	18.164	14.430	14.442	22.176	22.242
			2	26.386	26.413	25.886	25.888	22.941	22.956	29.410	29.457
			3	43.260	43.332	42.738	42.734	39.956	40.020	46.293	46.380
	0.17	10	1	18.216	18.776	17.904	18.416	15.279	15.577	20.089	20.847
			2	26.828	27.499	26.671	27.316	24.501	25.005	28.718	29.519
			3	42.135	43.675	41.834	43.399	39.772	41.180	44.262	45.938
		50	1	22.837	22.874	22.103	22.139	17.561	17.574	27.060	27.127
			2	33.050	33.080	32.515	32.547	28.664	28.680	37.090	37.139
			3	55.112	55.204	54.571	54.674	50.391	50.472	59.812	59.924
	0.28	10	1	20.691	21.498	20.640	21.373	17.549	17.995	23.004	24.033
			2	29.170	30.019	29.401	30.207	26.304	26.923	32.254	33.247
			3	44.903	46.607	45.412	47.128	42.055	43.558	48.975	50.908
		50	1	27.766	27.837	26.930	26.993	20.869	20.892	33.329	33.451
			2	37.466	37.515	37.094	37.142	31.174	31.194	43.775	43.859
			3	59.776	59.882	60.014	60.128	52.887	52.967	68.437	68.579
45°	0.12	10	1	16.146	16.980	15.927	16.691	14.275	14.729	17.307	18.414
			2	25.980	27.098	25.709	26.776	24.418	25.270	27.110	28.420
			3	38.426	41.352	37.814	40.494	36.576	38.974	39.621	42.828
		50	1	21.164	21.240	20.522	20.577	17.133	17.159	24.427	24.561
			2	34.553	34.647	33.713	33.749	30.876	30.925	37.679	37.821
			3	58.642	58.931	56.577	56.720	52.787	52.997	62.826	63.171
	0.17	10	1	20.351	21.297	20.119	20.974	17.843	18.350	22.059	23.324
			2	33.204	34.560	32.923	34.209	30.958	31.996	35.091	36.680
			3	49.239	52.877	48.510	51.762	46.516	49.257	51.341	55.373
		50	1	26.069	26.148	25.320	25.388	21.086	21.111	30.201	30.339
			2	43.647	43.753	42.654	42.747	38.708	38.762	48.133	48.294
			3	74.457	74.814	71.677	72.004	65.984	66.223	81.139	81.580
	0.28	10	1	22.578	23.935	22.730	23.950	19.835	20.603	24.941	26.639
			2	35.630	37.291	35.982	37.537	32.968	34.212	38.991	40.939
			3	52.467	56.634	52.827	56.658	49.821	53.250	56.380	61.081
		50	1	30.807	30.951	30.120	30.241	24.154	24.202	36.545	36.788
			2	48.378	48.536	47.874	48.010	41.548	41.621	55.836	56.083
			3	81.232	81.652	79.909	80.306	71.204	71.482	92.735	93.307
30°	0.12	10	1	22.026	23.037	21.874	22.764	20.556	21.132	23.076	24.369
			2	35.790	38.414	35.393	37.696	34.218	36.220	36.920	39.851
			3	48.488	53.298	48.046	52.222	46.768	50.579	49.692	54.883
		50	1	29.557	29.680	28.675	28.721	25.707	25.717	32.750	32.979
			2	55.280	55.701	52.700	52.908	48.992	49.207	59.842	60.416
			3	87.659	88.906	82.247	82.849	75.991	76.537	95.834	97.611
	0.17	10	1	28.110	29.262	28.022	29.010	26.010	26.665	29.843	31.308
			2	45.913	49.113	45.515	48.262	43.560	45.975	47.942	51.523
			3	62.291	68.209	61.882	66.916	59.703	64.333	64.532	70.928
		50	1	37.066	37.185	36.074	36.135	32.087	32.075	41.427	41.663
			2	69.851	70.336	66.559	66.906	61.164	61.388	76.758	77.446
			3	110.133	111.529	103.367	104.241	94.491	95.031	122.063	124.135
	0.28	10	1	30.267	31.889	30.870	32.269	27.752	28.780	33.281	35.161
			2	48.805	52.635	49.540	52.880	46.258	49.343	52.755	56.928
			3	65.977	72.898	67.116	73.145	63.538	69.423	70.563	77.795
		50	1	41.856	42.098	41.319	41.478	35.068	35.121	48.609	49.020
			2	77.179	77.849	74.931	75.438	66.601	66.936	88.338	89.322
			3	123.376	125.438	117.376	118.770	104.682	105.621	141.233	144.254

Table 9: Comparison study of frequency parameter λ_1 of skew plates with CCCC boundary conditions ($a/b = 1, \varphi = 0^\circ$)

Skew angle	ν_{CNT}	b/t	Mode	Types							
				UD		FG - V		FG - O		FG - X	
				Present	ANSYS	Present	ANSYS	Present	ANSYS	Present	ANSYS
90°	0.12	10	1	20.369	20.448	19.484	19.564	18.623	18.701	21.148	21.229
			2	25.232	25.510	24.633	24.906	23.786	24.054	26.051	26.333
			3	34.791	35.396	34.491	35.089	33.608	34.209	35.707	36.311
		50	1	38.054	38.049	32.419	32.411	28.592	28.587	44.892	44.886
			2	42.630	42.602	37.808	37.761	34.246	34.229	49.057	49.024
			3	54.329	54.313	50.860	50.781	47.515	47.526	60.131	60.102
	0.17	10	1	25.876	25.977	24.677	24.780	23.438	23.540	27.107	27.210
			2	32.267	32.622	31.516	31.865	30.181	30.526	33.683	34.042
			3	44.724	45.500	44.451	45.222	42.927	43.708	46.445	47.215
		50	1	46.185	46.176	39.214	39.218	34.523	34.517	54.736	54.729
			2	52.448	52.416	46.644	46.630	42.076	42.057	60.652	60.616
			3	68.167	68.154	64.227	64.254	59.471	59.487	76.050	76.024
	0.28	10	1	28.134	28.242	27.543	27.653	26.259	26.370	29.863	29.972
			2	34.559	34.939	34.458	34.835	32.617	32.999	37.063	37.444
			3	47.333	48.156	47.882	48.708	45.300	46.166	50.929	51.731
		50	1	56.485	56.478	48.048	48.052	42.208	42.201	66.975	66.966
			2	62.123	62.080	54.966	54.945	48.674	48.642	72.979	72.938
			3	76.975	76.940	72.173	72.178	64.593	64.585	89.067	89.033
60°	0.12	10	1	20.995	21.788	20.341	20.976	19.572	20.118	21.705	22.582
			2	28.505	29.006	28.071	28.465	27.235	27.588	29.333	29.876
			3	39.664	40.584	39.259	40.118	38.313	39.136	40.634	41.594
		50	1	39.016	39.367	33.764	33.949	30.082	30.205	45.494	46.091
			2	46.953	47.203	42.731	42.814	39.258	39.328	52.952	53.409
			3	64.299	64.483	61.212	61.193	57.590	57.658	69.937	70.272
	0.17	10	1	26.783	27.735	25.917	26.651	24.756	25.392	27.967	29.016
			2	36.563	37.159	36.056	36.508	34.675	35.099	38.064	38.691
			3	50.972	52.128	50.546	51.622	48.951	49.992	52.775	53.981
		50	1	47.613	47.976	41.137	41.339	36.552	36.674	55.806	56.431
			2	58.320	58.566	53.282	53.405	48.632	48.697	66.220	66.677
			3	81.248	81.435	77.704	77.819	72.291	72.361	89.366	89.699
	0.28	10	1	28.835	30.017	28.570	29.552	27.190	28.128	30.741	31.948
			2	38.887	39.640	39.105	39.716	36.993	37.662	41.814	42.492
			3	53.974	55.258	54.567	55.781	51.980	53.203	57.729	59.042
		50	1	57.446	58.103	49.673	50.034	43.827	44.058	67.649	68.698
			2	67.463	67.951	61.422	61.669	54.708	54.856	78.489	79.292
			3	90.041	90.400	86.305	86.503	77.569	77.692	103.276	103.859
45°	0.12	10	1	23.964	24.796	23.508	24.099	22.757	23.240	24.685	25.622
			2	34.715	35.123	34.332	34.580	33.439	33.639	35.614	36.080
			3	46.055	47.343	45.525	46.420	44.505	45.327	47.089	48.441
		50	1	42.216	42.823	37.542	37.851	34.005	34.208	48.288	49.334
			2	56.919	57.343	53.263	53.396	49.624	49.737	62.666	63.430
			3	83.101	83.549	79.404	79.513	74.587	74.805	89.449	90.149
	0.17	10	1	30.698	31.660	30.133	30.764	28.919	29.454	31.980	33.041
			2	44.599	45.049	44.184	44.417	42.677	42.894	46.269	46.753
			3	59.161	60.649	58.598	59.543	56.889	57.857	61.080	62.529
		50	1	52.012	52.636	46.304	46.635	41.746	41.944	59.866	60.947
			2	71.468	71.889	67.115	67.310	61.937	62.038	79.478	80.243
			3	105.291	105.782	100.642	100.986	93.369	93.600	114.986	115.740
	0.28	10	1	32.739	34.028	32.814	33.789	31.094	32.112	35.129	36.328
			2	47.262	47.921	47.740	48.180	45.321	45.896	50.700	51.208
			3	62.687	64.676	63.290	64.809	60.688	62.663	66.746	68.223
		50	1	61.307	62.454	54.538	55.145	48.411	48.812	71.557	73.371
			2	80.429	81.257	75.674	76.083	67.824	68.082	92.560	93.880
			3	115.650	116.436	111.939	112.446	100.892	101.240	131.718	132.896
30°	0.12	10	1	34.495	33.701	34.256	33.209	33.409	32.346	35.345	34.585
			2	48.763	48.048	48.420	47.397	47.403	46.340	49.794	49.155
			3	61.579	61.752	61.212	60.933	60.130	59.729	62.660	62.978
		50	1	55.686	56.248	52.027	52.195	48.440	48.528	61.383	62.441
			2	85.944	86.435	81.829	81.834	76.799	76.834	92.771	93.672
			3	123.356	124.589	116.680	116.894	109.135	109.356	133.297	135.273
	0.17	10	1	44.376	43.231	44.176	42.681	42.684	41.282	46.016	44.803
			2	62.740	61.673	62.447	60.947	60.679	59.257	64.731	63.643
			3	79.264	79.280	78.986	78.364	77.110	76.468	81.393	81.479
		50	1	69.859	70.391	65.521	65.688	60.453	60.493	77.763	78.795
			2	108.721	109.190	103.641	103.736	96.163	96.126	119.008	119.903
			3	155.705	156.958	147.286	147.688	136.329	136.393	170.612	172.743
	0.28	10	1	46.875	45.967	47.537	46.258	44.969	44.138	50.460	49.006
			2	66.249	65.481	67.215	65.999	64.235	63.505	70.664	69.377
			3	83.593	84.109	84.946	84.851	81.843	82.213	88.504	88.541
		50	1	78.752	79.895	73.941	74.436	66.272	66.584	90.583	92.407
			2	119.894	120.880	115.512	115.943	104.105	104.373	136.520	138.049
			3	172.463	174.709	165.228	166.406	149.274	150.027	195.486	198.796

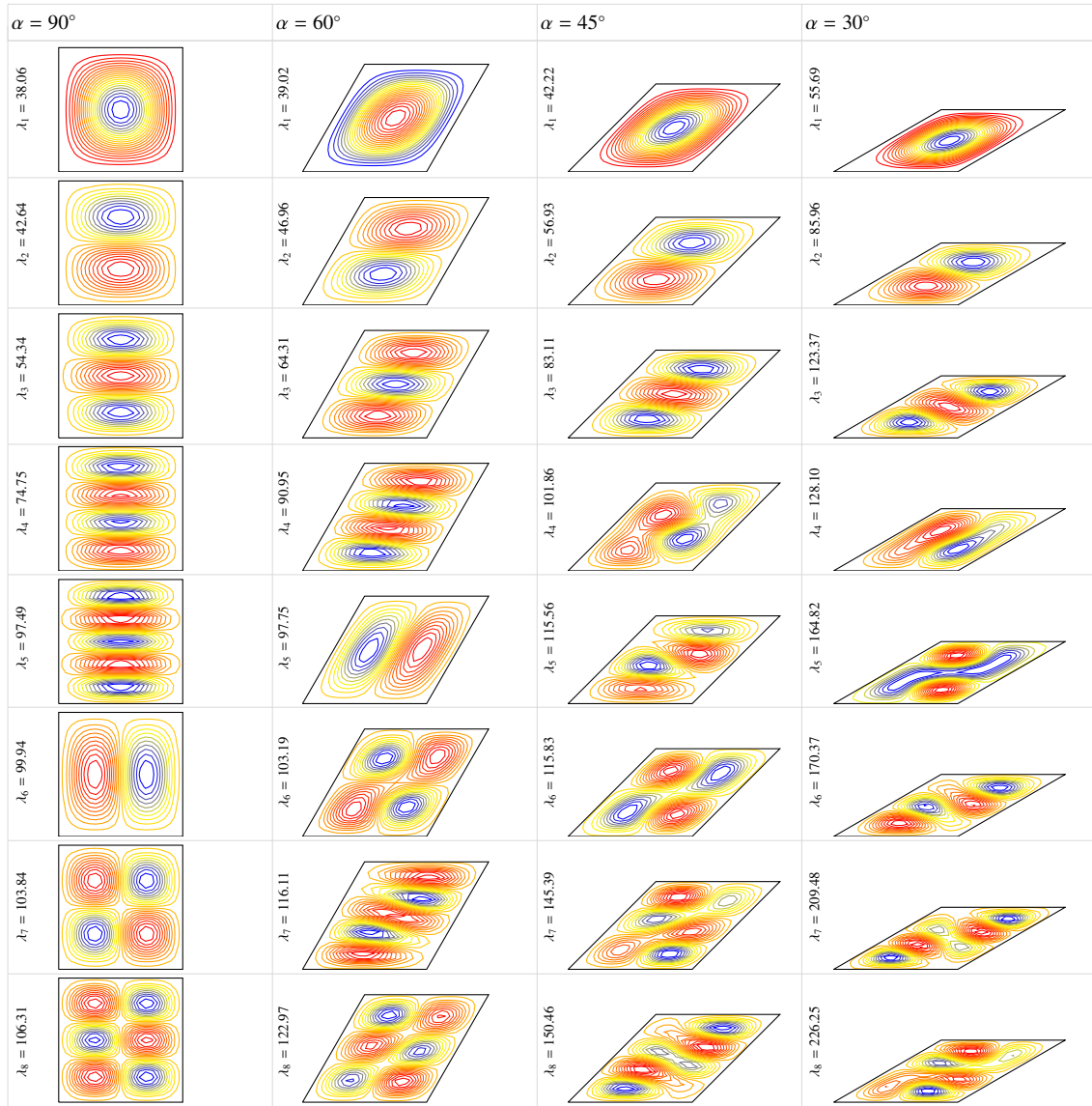


Figure 11: First eight mode shapes of a fully clamped UD-CNTRC skew plate for skew angles $\alpha = 90^\circ, 60^\circ, 45^\circ$ and 30° , $V_{CNT}^* = 12\%$, $a/b = 1$, $t/b = 0.02$ and $\varphi = 0^\circ$.

importance of taking into consideration the direction of the CNTs in order to optimize the mechanical response of the FG-CNTRC skew plates. For example, with a skew angle of $\alpha = 30^\circ$ and SSSS boundary conditions, the variation of the φ may increase the first frequency parameter by up to 11.7% and decrease it by up to 18.6%.

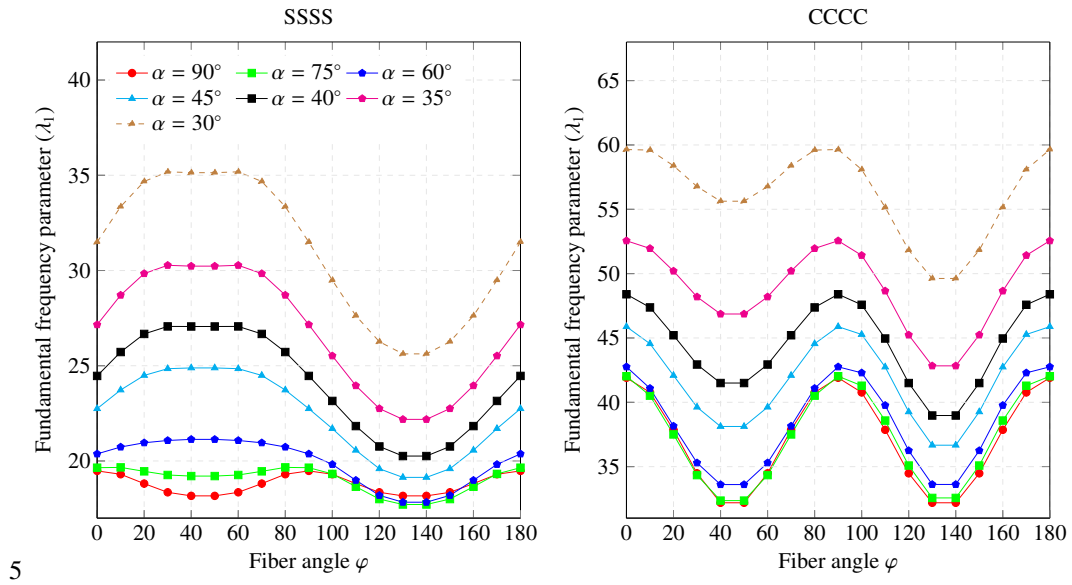


Figure 12: Effect of fiber angle φ on the first frequency parameter λ_1 of a CNTRC skew plate (UD-CNTRC, $V_{CNT} = 12\%$, $a/b = 1$, $b/t = 50$).

5. Conclusions

In this paper, static and free vibration analyses of moderately thick FG-CNTRC skew plates are presented. An efficient finite element formulation based on the Hu-Washizu principle is presented. The shell theory is formulated in oblique coordinates and includes the effects of transverse shear strains by first-order shear deformation theory (FSDT). An invariant definition of the elastic transversely isotropic tensor based on the representation theorem is defined in oblique coordinates. Independent approximations of displacements (bilinear), strains and stresses (piecewise constant within subregions) provide a consistent mechanism to formulate four-noded skew elements with a total number of twenty degrees of freedom. A set of eigenvalue equations for the FG-CNTRC skew plate vibration is derived, from which the natural frequencies and mode shapes can be obtained. Detailed parametric studies have been carried out to investigate the influences of skew angle, carbon nanotube volume fraction, plate thickness-to-width ratio, plate aspect ratio, boundary condition and distribution profile of reinforcements (uniform and three non-uniform distributions) on the static and free vibration characteristics of the FG-CNTRC skew plates. The results are compared to commercial code ANSYS and limited existing bibliography with very good agreement.

Acknowledgement

This research was supported by Spanish ministry of economy and competitively under the Project Ref: DPI2014-53947-R. E. G-M was also supported by a FPU contract-fellowship from the Spanish Ministry of Education Ref: FPU13/04892.

References

- [1] S. Iijima, Helical microtubules of graphitic carbon, *Nature (London, United Kingdom)* 354 (1991) 56–58.
- [2] R. F. Gibson, A review of recent research on mechanics of multifunctional composite materials and structures, *Composite structures* 92 (2010) 2793–2810.
- [3] A. M. Esawi, M. M. Farag, Carbon nanotube reinforced composites: potential and current challenges, *Materials & design* 28 (2007) 2394–2401.
- [4] L. Zhang, Z. Lei, K. Liew, Vibration characteristic of moderately thick functionally graded carbon nanotube reinforced composite skew plates, *Composite Structures* 122 (2015) 172–183.
- [5] J. Wuite, S. Adali, Deflection and stress behaviour of nanocomposite reinforced beams using a multiscale analysis, *Composite structures* 71 (2005) 388–396.
- [6] T. Vodenitcharova, L. Zhang, Bending and local buckling of a nanocomposite beam reinforced by a single-walled carbon nanotube, *International Journal of Solids and Structures* 43 (2006) 3006–3024.
- [7] G. Formica, W. Lacarbonara, R. Alessi, Vibrations of carbon nanotube-reinforced composites, *Journal of Sound and Vibration* 329 (2010) 1875–1889.
- [8] A. G. Arani, S. Maghamikia, M. Mohammadimehr, A. Arefmanesh, Buckling analysis of laminated composite rectangular plates reinforced by swcnts using analytical and finite element methods, *Journal of Mechanical Science and Technology* 25 (2011) 809–820.
- [9] H. Rokni, A. S. Milani, R. J. Seethaler, 2d optimum distribution of carbon nanotubes to maximize fundamental natural frequency of polymer composite micro-beams, *Composites Part B: Engineering* 43 (2012) 779–785.
- [10] G. Udupa, S. S. Rao, K. Gangadharan, Functionally graded composite materials: An overview, *Procedia Materials Science* 5 (2014) 1291–1299.
- [11] H.-S. Shen, Nonlinear bending of functionally graded carbon nanotube-reinforced composite plates in thermal environments, *Composite Structures* 91 (2009) 9–19.
- [12] K. Liew, Z. Lei, L. Zhang, Mechanical analysis of functionally graded carbon nanotube reinforced composites: a review, *Composite Structures* 120 (2015) 90–97.

- [13] P. Zhu, Z. Lei, K. M. Liew, Static and free vibration analyses of carbon nanotube-reinforced composite plates using finite element method with first order shear deformation plate theory, *Composite Structures* 94 (2012) 1450–1460.
- [14] L.-L. Ke, J. Yang, S. Kitipornchai, Nonlinear free vibration of functionally graded carbon nanotube-reinforced composite beams, *Composite Structures* 92 (2010) 676–683.
- [15] P. Zhu, L. Zhang, K. Liew, Geometrically nonlinear thermomechanical analysis of moderately thick functionally graded plates using a local petrov-galerkin approach with moving kriging interpolation, *Composite Structures* 107 (2014) 298–314.
- [16] H.-S. Shen, C.-L. Zhang, Thermal buckling and postbuckling behavior of functionally graded carbon nanotube-reinforced composite plates, *Materials & Design* 31 (2010) 3403–3411.
- [17] B. Sobhani Aragh, A. Nasrollah Barati, H. Hedayati, Eshelby-mori-tanaka approach for vibrational behavior of continuously graded carbon nanotube-reinforced cylindrical panels, *Composites Part B: Engineering* 43 (2012) 1943–1954.
- [18] M. Yas, M. Heshmati, Dynamic analysis of functionally graded nanocomposite beams reinforced by randomly oriented carbon nanotube under the action of moving load, *Applied Mathematical Modelling* 36 (2012) 1371–1394.
- [19] M. Heshmati, M. Yas, Vibrations of non-uniform functionally graded mwcnts-polystyrene nanocomposite beams under action of moving load, *Materials & Design* 46 (2013) 206–218.
- [20] A. Alibeigloo, K. Liew, Thermoelastic analysis of functionally graded carbon nanotube-reinforced composite plate using theory of elasticity, *Composite Structures* 106 (2013) 873–881.
- [21] A. Alibeigloo, A. Emtehani, Static and free vibration analyses of carbon nanotube-reinforced composite plate using differential quadrature method, *Meccanica* 50 (2015) 61–76.
- [22] L. Zhang, Z. Song, K. Liew, State-space levy method for vibration analysis of fg-cnt composite plates subjected to in-plane loads based on higher-order shear deformation theory, *Composite Structures* 134 (2015) 989–1003.
- [23] C.-P. Wu, H.-Y. Li, Three-dimensional free vibration analysis of functionally graded carbon nanotube-reinforced composite plates with various boundary conditions, *Journal of Vibration and Control* (2014) 362–370.
- [24] P. Malekzadeh, A. Zarei, Free vibration of quadrilateral laminated plates with carbon nanotube reinforced composite layers, *Thin-Walled Structures* 82 (2014) 221–232.
- [25] L. Zhang, D. Li, K. Liew, An element-free computational framework for elastodynamic problems based on the imls-ritz method, *Engineering Analysis with Boundary Elements* 54 (2015) 39–46.
- [26] L. Zhang, D. Huang, K. Liew, An element-free imls-ritz method for numerical solution of three-dimensional wave equations, *Computer Methods in Applied Mechanics and Engineering* 297 (2015) 116–139.
- [27] L. Zhang, P. Zhu, K. Liew, Thermal buckling of functionally graded plates using a local kriging meshless method, *Composite Structures* 108 (2014) 472–492.
- [28] Z. Lei, L. Zhang, K. Liew, J. Yu, Dynamic stability analysis of carbon nanotube-reinforced functionally graded cylindrical panels using the element-free kp-ritz method, *Composite Structures* 113 (2014) 328–338.
- [29] Z. Lei, L. Zhang, K. Liew, Free vibration analysis of laminated FG-CNT reinforced composite rectangular plates using the kp-ritz method, *Composite Structures* 127 (2015) 245–259.
- [30] L. Zhang, Z. Lei, K. Liew, Buckling analysis of FG-CNT reinforced composite thick skew plates using an element-free approach, *Composites Part B: Engineering* 75 (2015) 36–46.
- [31] L. Zhang, K. Liew, J. Reddy, Postbuckling of carbon nanotube reinforced functionally graded plates with edges elastically restrained against translation and rotation under axial compression, *Computer Methods in Applied Mechanics and Engineering* 298 (2016) 1–28.

- [32] L. Zhang, Z. Lei, K. Liew, An element-free IMLS-Ritz framework for buckling analysis of FG-CNT reinforced composite thick plates resting on winkler foundations, *Engineering Analysis with Boundary Elements* 58 (2015) 7–17.
- [33] L. Zhang, Z. Song, K. Liew, Nonlinear bending analysis of FG-CNT reinforced composite thick plates resting on Pasternak foundations using the element-free IMLS-Ritz method, *Composite Structures* 128 (2015) 165–175.
- [34] L. Zhang, Z. Lei, K. Liew, Free vibration analysis of functionally graded carbon nanotube-reinforced composite triangular plates using the fsdt and element-free IMLS-Ritz method, *Composite Structures* 120 (2015) 189–199.
- [35] L. Zhang, Z. Lei, K. Liew, J. Yu, Static and dynamic of carbon nanotube reinforced functionally graded cylindrical panels, *Composite Structures* 111 (2014) 205–212.
- [36] Z. Lei, L. Zhang, K. Liew, Vibration analysis of CNT-reinforced functionally graded rotating cylindrical panels using the element-free kp-ritz method, *Composites Part B: Engineering* 77 (2015) 291–303.
- [37] E. A. Shahrbabaki, A. Alibeigloo, Three-dimensional free vibration of carbon nanotube-reinforced composite plates with various boundary conditions using ritz method, *Composite Structures* 111 (2014) 362–370.
- [38] L. Zhang, Z. Lei, K. Liew, Computation of vibration solution for functionally graded carbon nanotube-reinforced composite thick plates resting on elastic foundations using the element-free imls-ritz method, *Applied Mathematics and Computation* 256 (2015) 488–504.
- [39] A. Leissa, *Plate vibration research, 1976-1980: classical theory* (1981).
- [40] A. Leissa, *Recent studies in plate vibrations, 1981-1985, part i: classical theory* (1987).
- [41] K. Liew, Y. Xiang, S. Kitipornchai, Research on thick plate vibration: a literature survey, *Journal of Sound and Vibration* 180 (1995) 163–176.
- [42] O. McGee, J. Kim, Y. Kim, Corner stress singularity effects on the vibration of rhombic plates with combinations of clamped and simply supported edges, *Journal of Sound and Vibration* 193 (1996) 555–580.
- [43] Z. Lei, L. Zhang, K. Liew, Buckling of FG-CNT reinforced composite thick skew plates resting on pasternak foundations based on an element-free approach, *Applied Mathematics and Computation* 266 (2015) 773–791.
- [44] L. Zhang, K. Liew, Large deflection analysis of FG-CNT reinforced composite skew plates resting on pasternak foundations using an element-free approach, *Composite Structures* 132 (2015) 974–983.
- [45] D.-L. Shi, X.-Q. Feng, Y. Y. Huang, K.-C. Hwang, H. Gao, The effect of nanotube waviness and agglomeration on the elastic property of carbon nanotube-reinforced composites, *Journal of Engineering Materials and Technology* 126 (2004) 250–257.
- [46] J. Fidelus, E. Wiesel, F. Gojny, K. Schulte, H. Wagner, Thermo-mechanical properties of randomly oriented carbon/epoxy nanocomposites, *Composites Part A: Applied Science and Manufacturing* 36 (2005) 1555–1561.
- [47] G. Wempner, D. Talaslidis, *Mechanics of Solids and Shells*, CRC Press, 2003.
- [48] A. Spencer, The formulation of constitutive equation for anisotropic solids, in: *Mechanical Behavior of Anisotropic Solids/Comportment Mchanique des Solides Anisotropes*, Springer, 1982, pp. 3–26.
- [49] V. Lubarda, M. Chen, On the elastic moduli and compliances of transversely isotropic and orthotropic materials, *Journal of Mechanics of Materials and Structures* 3 (2008) 153–171.
- [50] E. Efraim, M. Eisenberger, Exact vibration analysis of variable thickness thick annular isotropic and fgm plates, *Journal of Sound and Vibration* 299 (2007) 720–738.
- [51] D. Talaslidis, G. Wempner, The linear isoparametric triangular element: theory and application, *Computer Methods in Applied Mechanics and Engineering* 103 (1993) 375–397.
- [52] G. Wempner, A. Talaslidis, C. Hwang, A simple and efficient approximation of shells via quadrilateral elements, *Journal of Applied Mechanics* 49 (1982) 115–120.

- [53] S. Wolfram, *Mathematica*, 4th edition, Wolfram Media (1999).
- [54] K. Liew, Y. Xiang, S. Kitipornchai, C. Wang, Vibration of thick skew plates based on mindlin shear deformation plate theory, *Journal of Sound and Vibration* 168 (1993) 39–69.
- [55] C. Huang, A. Leissa, M. Chang, Vibrations of skewed cantilevered triangular, trapezoidal and parallelogram mindlin plates with considering corner stress singularities, *International Journal for Numerical Methods in Engineering* 62 (2005) 1789–1806.
- [56] Y. Han, J. Elliott, Molecular dynamics simulations of the elastic properties of polymer/carbon nanotube composites, *Computational Materials Science* 39 (2007) 315–323.